Direct and indirect climate change effects on carbon dioxide fluxes in a thawing boreal forest-wetland landscape

Manuel Helbig[1]*, Laura E Chasmer[2], Ankur R Desai[3], Natascha Kljun[4], William L Quinton[5], Oliver Sonnentag[1]

[1]*Université de Montréal*
Département de géographie & Centre d'études nordiques
520 Chemin de la Côte Sainte-Catherine
Montréal, QC H2V 2B8, Canada

[2]*University of Lethbridge, Department of Geography, Lethbridge AB T1K 3M4, Canada*

[3]*University of Wisconsin-Madison, Department of Atmospheric and Oceanic Sciences, Madison, WI 53706, USA*

[4]*Swansea University, Department of Geography, Singleton Park, Swansea SA28PP, UK*

[5]*Wilfrid Laurier University, Cold Regions Research Centre, Waterloo ON N2L 3C5, Canada*

*corresponding author:
tel. 438-826-1985
fax 514 343-8008
email: manuel.helbig@umontreal.ca

Keywords: Climate change, Eddy covariance, Carbon dioxide, Boreal forest, Wetlands, Gross primary productivity, Ecosystem respiration, Permafrost

Running head: *Climate impacts on NEE in boreal landscapes*
Submitted to: *Global Change Biology*
Primary Research Article

Abstract

In the sporadic permafrost zone of northwestern Canada, boreal forest carbon dioxide (CO_2) fluxes will be altered directly by climate change through changing meteorological forcing and indirectly through changes in landscape functioning associated with thaw-induced collapse-scar bog ("wetland") expansion. However, their combined effect on landscape-scale net ecosystem CO_2 exchange (NEE_{LAND}), resulting from changing gross primary productivity (GPP) and ecosystem respiration (ER), remains unknown. Here, we quantify indirect land cover change impacts on NEE_{LAND} and direct climate change impacts on modeled temperature- and light-limited NEE_{LAND} of a boreal forest-wetland landscape. Using nested eddy covariance flux towers, we find both GPP and ER to be larger at the landscape- compared to the wetland-level. However, annual NEE_{LAND} (-20 g C m^{-2}) and wetland NEE (-24 g C m^{-2}) were similar, suggesting negligible wetland expansion effects on NEE_{LAND}. In contrast, we find non-negligible direct climate change impacts when modeling NEE_{LAND} using projected air temperature and incoming shortwave radiation. At the end of the 21st century, modeled GPP mainly increases in spring and fall due to reduced temperature-limitation, but becomes more frequently light-limited in fall. In a warmer climate, ER increases year-round in the absence of moisture stress resulting in net CO_2 uptake increases in the shoulder seasons and decreases during the summer. Annually, landscape net CO_2 uptake is projected to decline by 25±14 g C m^{-2} for a moderate and 103±38 g C m^{-2} for a high warming scenario, potentially reversing recently observed positive net CO_2 uptake trends across the boreal biome. Thus, even without moisture stress, net CO_2 uptake of boreal forest-wetland landscapes may decline, and ultimately these landscapes may turn into net CO_2 sources under continued anthropogenic CO_2 emissions. We conclude that NEE_{LAND} changes

62 are more likely to be driven by direct climate change rather than by indirect land cover change
63 impacts.
64
65 **Introduction**
66 The boreal biome, with its distinct land-atmosphere exchange of sensible heat, water
67 vapor, methane, and carbon dioxide (CO_2), plays an important role in the global and regional
68 climate systems (Chapin *et al.*, 2000). For example, boreal forests represent an important carbon
69 (C) sink of about 0.5 Pg C yr^{-1} (Pan *et al.*, 2011), equivalent to 17±6 % of the global land CO_2
70 sink (Le Quéré *et al.*, 2015). Climate warming in the boreal biome of northwestern North
71 America has caused widespread permafrost thaw at the southern permafrost limit inducing
72 wetland expansion leading to replacement of boreal forests in lowland regions (e.g.; Helbig *et*
73 *al.*, 2016a; Lara *et al.*, 2016; Chasmer & Hopkinson, in press). Previous studies have shown that
74 land cover changes in these regions affect regional land-atmosphere interactions by favoring the
75 partitioning of available energy to latent instead of sensible heat (Helbig *et al.*, 2016b) and by
76 enhancing landscape methane emissions (Helbig *et al.*, in press). However, it remains uncertain
77 how climate warming and resulting land cover changes influence net ecosystem CO_2 exchange
78 (NEE), and its component fluxes gross primary productivity (GPP) and ecosystem respiration
79 (ER) (Schuur *et al.*, 2015).
80 Along the southern limit of the North American permafrost zone, long-term net CO_2
81 uptake has resulted in large organic C stocks as peat (Robinson & Moore, 1999; Tarnocai *et al.*,
82 2009; Treat *et al.*, 2016). In these organic-rich boreal landscapes, thawing permafrost makes
83 previously frozen organic C stocks available for decomposition and ER may be enhanced by
84 warming soils (Schuur *et al.*, 2009; O'Donnell *et al.*, 2012; Natali *et al.*, 2014; Treat *et al.*, 2014;

85 Koven *et al.*, 2015). However, permafrost thaw in organic- and ice-rich landscapes often leads to
86 surface subsidence and increased land surface wetness (e.g.; Osterkamp *et al.*, 2000; Baltzer *et*
87 *al.*, 2014). Under saturated and anoxic conditions, associated with subsidence, organic matter
88 decomposes more slowly, causing only an attenuated post-thaw increase in ER (Knoblauch *et al.*,
89 2013). At the same time, GPP might increase due to increased nutrient and soil moisture
90 availability, and warmer soil and air temperatures (e.g.; Turetsky *et al.*, 2000; Camill *et al.*, 2001;
91 Wickland *et al.*, 2006; Turetsky *et al.*, 2007; Keuper *et al.*, 2012; Finger *et al.*, 2016). The
92 combination of changes in both GPP and ER in a warming climate will eventually determine if
93 organic-rich boreal landscapes will continue to be long-term CO_2 sinks exerting a climate
94 cooling effect (Frolking *et al.*, 2006). Since 1985, the land net CO_2 sink in the boreal biome (50°
95 to 60° N, excluding Europe) increased by 8-11 Tg C yr^{-1} (Welp *et al.*, 2016), but it remains
96 unclear if this trend will continue in an increasingly warmer climate.

97 Recent warming trends in northwestern Canada, in the order of 0.25-0.50 °C per decade
98 (DeBeer *et al.*, 2016), are likely to continue and potentially accelerate during the 21st century
99 (Kirtman *et al.*, 2013). Direct climate change effects result from instantaneous ecosystem
100 responses to these altered meteorological conditions. For example, boreal forest GPP is
101 suppressed at air temperatures (T_a, °C) below the freezing point and increases with both T_a- and
102 light-availability (Tanja *et al.*, 2003; Luyssaert *et al.*, 2007), while ER increases with T_a and soil
103 temperature (T_s, °C) (Dunn *et al.*, 2007; Ueyama *et al.*, 2014). In addition to substantially
104 warmer regional climates at high latitudes, future changes in cloud cover could alter incoming
105 shortwave radiation (SW_{in}, W m^{-2}) in these regions (Kirtman *et al.*, 2013). In contrast, indirect
106 climate change impacts result from changes in ecosystem composition, structure, and function
107 thus altering how ecosystems may respond to variations in meteorological conditions. For

example, a gradual increase in the temperature sensitivity of ER over several years can alter NEE of boreal forests in the absence of any warming trend (e.g., Hadden & Grelle, 2016). The abrupt vegetation changes following permafrost thaw in lowland boreal forests may trigger shifts in ecosystem function (Camill *et al.*, 2001). Thus, both direct and indirect climate change effects on GPP and ER need to be assessed to better constrain the future NEE of organic-rich boreal landscapes in the permafrost zone.

Here, we examine the direct climate change effects of altered meteorological conditions and the indirect effects of thaw-induced wetland expansion on NEE and its component fluxes GPP and ER for a boreal forest-wetland landscape in a rapidly thawing lowland region at the southern limit of permafrost in northwestern Canada (Quinton *et al.*, 2011; Baltzer *et al.*, 2014). We use nested eddy covariance net CO_2 flux measurements to compare NEE of the thawing landscape to NEE of a nearby permafrost-free wetland within the heterogeneous landscape, both exposed to the same meteorological conditions. Downscaled regional climate projections are used to assess the GPP, ER, and NEE response to a changing climate. We analyse

(i) how thaw-induced wetland expansion and associated forest loss indirectly affect NEE, GPP, and ER of the boreal forest-wetland landscape, and

(ii) how these indirect climate change effects compare to direct effects of projected changes in T_a and SW_{in} over the 21st century.

Materials and Methods

Study site

Scotty Creek (61°18' N; 121°18' W) is a 152-km^2 watershed in the sporadic permafrost zone (10-50% of land area underlain by permafrost) near Fort Simpson, NT in the southern Taiga Plains of northwestern Canada. With 70 Pg of soil organic C in the top 3 meters, the Taiga Plains store about 15 % of the total organic C stocks (<3 m) in the North American permafrost zone (data from Hugelius *et al.*, 2013). The dry continental climate of the Fort Simpson region is characterized by a mean T_a of -2.8 °C and a mean total precipitation of 388 mm with 149 mm falling as snow (1981-2010; Environment Canada, 2014). The southern part of Scotty Creek is characterized by a mosaic of forested permafrost (peat) plateaus, wetlands, forested uplands and shallow lakes (Chasmer *et al.*, 2014). Permafrost-free wetlands ("wetlands") occur mainly as collapse-scar bogs dominated by bryophytes (*Sphagnum balticum* and *S. magellanicum*), ericaceous shrubs (*Chamaedaphne calyculata*, *Andromeda polifolia*, *Vaccinium oxycoccos*), pod grass (*Scheuchzeria palustris*), and a few isolated black spruce (*Picea mariana*) and tamarack (*Larix laricina*). In contrast, forested permafrost plateaus ("forests") are characterized by a denser overstorey of black spruce with a shrub understorey and a ground cover comprising ericaceous shrubs (mainly *Rhododendron groenlandicum*), and lichens (*Cladonia* spp.) and bryophythes (*Sphagnum fuscum* and *S. capillifolium*), respectively (Garon-Labrecque *et al.*, 2015). Abiotic and biotic characteristics change abruptly between these two ecosystem types as indicated by contrasting overstorey leaf area index ($\geq$ 1 vs. $\leq$ 0.5 for forest and wetland, respectively) and soil moisture conditions ($\leq$ 30 % for the forests compared to $\geq$ 70 % for the wetlands). An active layer (i.e., seasonally thawed surface soil) of approximately 50 cm overlays near-surface permafrost in the forests. No near-surface permafrost is present in the wetlands

150 (Baltzer *et al.*, 2014). These changes occur over several meters across transition zones with
151 inundated, warmer peat soils (Bubier *et al.*, 1995; Baltzer *et al.*, 2014; Fig. 1). Warm soils in the
152 wetlands cause lateral thawing of near-surface permafrost underlying the forests and, thus, a
153 rapid expansion of permafrost-free wetlands (Kurylyk *et al.*, 2016). At Scotty Creek, forests and
154 wetlands comprise thick organic peat soils of ≥3 m with a mean total organic C content of
155 167±11 kg C m^{-2} (n = 3; Pelletier *et al.*, in press). About 20 % of North America's boreal forests
156 grow in the circumpolar permafrost zone on ice-rich permafrost and thick overburden cover, and
157 are thus prone to thaw-induced surface subsidence and to forest loss in a warming climate
158 (Helbig *et al.*, 2016a; Olefeldt *et al.*, 2016).
159
160 **Eddy covariance measurements**
161 Eddy covariance net CO_2 flux measurements were conducted at a landscape tower at
162 15.2 m above the mean lichen-moss surface of the permafrost plateau (23 March 2015 to 30
163 August 2016) and at a nested wetland tower at 1.9 m above the mean moss surface (10 June 2015
164 to 30 August 2016). At the wetland and the landscape tower, high-frequency (10 Hz) fluctuations
165 of vertical wind velocity and sonic temperature were measured with a sonic anemometer
166 (CSAT3A, Campbell Scientific, Logan, UT) and CO_2 and water vapor densities with a co-
167 located open-path infrared gas analyzer (EC150, Campbell Scientific). At the beginning of the
168 study period (23 March 2015 to 16 August 2015), an enclosed infrared gas analyzer (LI-7200,
169 LI-COR Biosciences, Lincoln, NE) was used for CO_2 and water vapor density measurements at
170 the landscape tower. Differences in net CO_2 fluxes derived from the LI-7200 and the EC150
171 were less than 5 % and cumulative net CO_2 fluxes over 57 days differed by 8 % (Helbig *et al.*,
172 2016c). Net ecosystem CO_2 exchange for the landscape (NEE_{LAND}; μmol m^{-2} s^{-1}) and the wetland

tower (NEE_{WET}; µmol m^{-2} s^{-1}) was calculated as the sum of the turbulent net CO_2 flux and a storage term. The storage term was derived from half-hourly CO_2 concentration changes at the measurement heights. We follow the micrometeorological NEE convention where net landscape/ecosystem CO_2 uptake is indicated by a negative sign and net CO_2 release to the atmosphere by a positive sign. Net ecosystem CO_2 exchange was filtered for periods with insufficient turbulence using a landscape tower friction velocity threshold of 0.13 m s^{-1} (95 % confidence interval (CI): 0.10 – 0.21 m s^{-1}), derived according to Papale *et al.* (2006). The 95 % CI was derived by using 100 bootstrapped nighttime NEE time series as input. The same threshold was used for the wetland and the landscape tower as the wetland is nested in the landscape tower footprints (Fig. S1). All flux calculations were done using the EddyPro software (version 6.1.0, LI-COR Biosciences). A more detailed description of the instrumental setup and the flux processing procedure is given in Helbig *et al.* (2016b) and Helbig *et al.* (2016c). For the entire study period, 55 % (daytime: 68 %; nighttime: 39 %) and 43 % (daytime: 56 %; nighttime: 28 %) of NEE passed the quality control at the landscape and wetland tower, respectively.

Assessing indirect climate change impacts on CO_2 fluxes using nested eddy covariance fluxes

Footprint modeling

Half-hourly 2-D flux footprints for the wetland and the landscape tower (defined as half-hourly probability maps of flux contribution per unit area [% per m^2]) were obtained according to Kljun *et al.* (2015). The flux footprints were combined with a land cover classification map (Chasmer *et al.*, 2014), as described by Helbig *et al.* (2016b), to derive sums of half-hourly probabilities of flux contributions for individual land cover types (i.e., flux footprint

196 contributions from forests and wetlands; Fig. 1). Additionally, transition zones were delineated
197 based on aerial photographs as areas of wetland expansion (and thus of forest loss) since 1977
198 (see Chasmer *et al.*, 2010). Within a radius of 350 m around the landscaper tower, 21 % of the
199 land surface was classified as transition zone. Their flux footprint contributions were then
200 separately derived for each half-hourly flux measurement. Transition zones are part of the
201 wetland land cover type and their definition is to some extent arbitrary, as a reference year (here
202 1977, the first year of available aerial photography) is used to differentiate between gradual
203 transition zones and interior wetlands. As the half-hourly variability in transition zone
204 contribution was relatively small (standard deviation: 2 % for wetland tower and 5 % for
205 landscape tower), only their average flux footprint contribution to the two flux towers over the
206 entire study period was analyzed. Wetland NEE was discarded when forest contributions were
207 greater than 5 % and NEE_{LAND} was discarded when contributions from a nearby lake were larger
208 than 5 % (Fig. 1). On average, forest contributions to landscape tower footprints were 48 %
209 whereas wetlands contributed 50 % (48 % from bogs and 2 % from fens). The remaining
210 contributions originated from the nearby lake. The wetland tower was located in a collapse-scar
211 bog and wetlands within the landscape tower footprint consisted to >95% of collapse-scar bogs.
212 In the following, “wetlands” therefore refer to collapse-scar bogs. Fens represent a second
213 permafrost-free wetland ecosystem type covering about 12% of the entire Scotty Creek
214 watershed (Chasmer *et al.*, 2014). Similar to collapse-scar bogs, fens are expanding due to
215 permafrost thaw (Chasmer & Hopkinson, in press). Due to their differing hydrology, vegetation
216 composition, and nutrient availability, CO_2 flux dynamics of fens most likely differ from CO_2
217 flux dynamics of collapse-scar bogs (e.g.; Bubier, 1995; Yu, 2006; Treat *et al.*, 2016).
218

Flux partitioning

Gaps in NEE were filled using the marginal distribution sampling method (Reichstein *et al.*, 2005) with SW_{in}, T_a, and water vapor pressure deficit (VPD, kPa) as look-up table variables. We calculated annual NEE for 100 friction velocity thresholds (as derived from bootstrapped nighttime NEE) to derive the 95 % CI of annual NEE.

To partition NEE into its component fluxes, GPP (μmol m^{-2} s^{-1}) and ER (μmol m^{-2} s^{-1}), we used a bulk partitioning approach (e.g.; Runkle *et al.*, 2013). The non-gap-filled, half-hourly daytime NEE (SW_{in} > 5 W m^{-2}) was fit to a bulk model combining a rectangular hyperbola function (for GPP) and an empirical Q_{10} model (for ER):

$$NEE = -GPP + ER = \underbrace{-\frac{GPP_{max}\,\alpha\,SW_{in}}{GPP_{max}+\alpha\,SW_{in}}}_{Term\ A} + \underbrace{ER_{base}Q_{10}^{\frac{Ta-T_{ref}}{\gamma}}}_{Term\ B} \qquad (1)$$

where GPP_{max} (μmol m^{-2} s^{-1}) is the maximum canopy photosynthetic capacity, α (μmol m^{-2} s^{-1} per W m^{-2}) is the initial canopy quantum efficiency, ER_{base} (μmol m^{-2} s^{-1}) is the basal respiration at a reference temperature (T_{ref} = 15 °C), Q_{10} indicates the sensitivity of *ER* to T_a, and γ = 10 °C is a constant (e.g.; Mahecha *et al.*, 2010). For the Q_{10} model, we selected T_a measurements within the forest canopy at 2 m above the lichen-moss surface because T_a represents an integrated temperature measure for the landscape whereas soil temperature varies spatially (laterally and vertically) across the heterogeneous landscape (Helbig *et al.*, in press). We fixed the Q_{10} parameter in a first iteration (Q_{10} = 2.5 [landscape] and Q_{10} = 1.1 [wetland]) before deriving the final GPP_{max}, α, and ER_{base}, as described in Reichstein *et al.* (2005). To derive a complete *ER* time series, we combined gap-filled nighttime NEE (i.e., ER) with the modeled daytime ER (see Term B in Eqn. 1). Ecosystem respiration was then subtracted from measured NEE to derive GPP. By using only daytime NEE to obtain daytime ER, we account for

241 potential light inhibition of leaf respiration during the day (Wehr *et al.*, 2016) and avoid
242 problems of extrapolating relationships between nighttime T_a and ER to daytime conditions (e.g.,
243 Lasslop *et al.*, 2010). We assessed indirect land cover change impacts on CO_2 fluxes by
244 analysing differences between NEE and derived component fluxes from the two eddy covariance
245 flux towers with contrasting flux footprint composition.

246

247 ***Modeling NEE and GPP***

248 In this study, we assess how daily light- and temperature-conditions affect mean daily
249 NEE_{LAND}. Net ecosystem CO_2 exchange is the small difference between its two large component
250 fluxes GPP and ER. Ecosystem respiration is strongly controlled by temperature whereas light
251 and temperature are strong controls on GPP, highlighting the potentially different responses of
252 ER and GPP to changing climatic conditions (e.g., Fang & Moncrieff, 2001; Huxman *et al.*,
253 2003; Lafleur *et al.*, 2005). We therefore modeled light-regulation of GPP using the rectangular
254 hyperbola function in Eqn. 1 and used a downward regulation scalar [f (T_a) in Eqn. 2] to account
255 for temperature-limitation of GPP. Mean daily GPP was fitted to the following equation with the
256 *nlinfit* function in Matlab (version 8.6.0; The MathWorks, Natick, MA) using daily means of T_a
257 and SW_{in}:

258 $$GPP = f(T_a)\, x\, \frac{GPP_{max}\, \alpha\, SW_{in}}{GPP_{max} + \alpha\, SW_{in}} \qquad (2)$$

259 f (T_a) is implemented as a sigmoidal function ranging from 0 to 1 and accounts for
260 instantaneous temperature constraints using mean daily T_a and for seasonal temperature
261 constraints using a moving T_a average (i.e., average of seven preceding days, T_{a_week}; °C). The
262 T_{a_week} constraint accounts for seasonality in biological controls other than the instantaneous GPP
263 response to T_a, such as physiological activity (e.g., Rayment *et al.*, 2002) and thermal

acclimation (e.g., Gea-Izquierdo *et al.*, 2010). According to Liebig's law, we assume that only the more limiting factor controls GPP (e.g.; Yuan *et al.*, 2007):

$$f(T_a) = \min\left(\frac{1}{1+a^{(b-Ta)}}, \frac{1}{1+a^{(c-T_{a\_week})}}\right) \quad (3)$$

where *a, b,* and *c* are model coefficients. Additionally, we constructed an ER model (ER_{MOD}) by fitting a Q_{10}-model (term B in Eqn. 1 based on daily T_a) to mean daily ER. Modeled NEE (NEE_{MOD}) was calculated as the sum of GPP_{MOD} and ER_{MOD}. Thus, NEE_{MOD} only depends on the climatic controls T_a and SW_{in} and does not account for other environmental or biological limitations on NEE (e.g.; soil moisture limitations; Niu *et al.*, 2011; Peichl *et al.*, 2013). Model uncertainties were estimated based on 1000 bootstrapped GPP and ER time series.

To characterize how the potential of NEE_{LAND} (NEE_{POT}) responds to changes in thermal conditions, we defined NEE_{POT} as the most negative daily NEE_{LAND} for given daily T_a (i.e., NEE_{LAND} < 15 percentile per T_a bin with each bin containing 2.5 % of all data). Like NEE_{POT}, we defined the temperature controlled potential of GPP_{LAND} (GPP_{POT_Ta}) as the upper limit of daily GPP_{LAND} for a given daily T_a and T_{a_week}. To characterize the light control on the potential of GPP_{LAND} (GPP_{POT_SWin}), we defined GPP_{POT_SWin} as the upper limit of daily GPP_{LAND} for a given daily SW_{in}. Sigmoidal functions were then fitted to GPP_{POT_Ta} and GPP_{POT_SWin}:

$$GPP_{POT\_i} = \frac{k}{1+l^{(m-x_i)}} + n \quad (4)$$

where GPP_{POT_i} is modeled GPP_{POT} for the variable x_i (i.e., T_a/T_{a_week} and SW_{in}) and *k, m, n,* and *l* are model coefficients. We defined GPP_{POT} as temperature-limited if GPP_{POT_Ta} for the observed daily T_a or T_{a_week} was smaller than GPP_{POT_SWin} for the observed daily SW_{in}. For the opposite case, GPP_{POT} was light-limited. If differences in GPP_{POT_Ta} and GPP_{POT_SWin} were less than 10 %, we assumed that GPP_{POT} was co-limited by temperature and light.

287 **Assessing direct climate change impacts on NEE**

288 To assess direct climate change impacts on NEE_{MOD}, GPP_{MOD}, and ER_{MOD}, we used the
289 modelling approach described above with regionally downscaled climate projections as drivers.
290 We obtained T_a and SW_{in} for the period 2006 to 2015 and 2091 to 2100 from the North
291 American Coordinated Regional Climate Downscaling Experiment (CORDEX;
292 http://www.cordex.org) and extracted daily time series for Scotty Creek. The CORDEX provides
293 downscaled climate projections at 50-km resolution for various combinations of Earth system
294 models (ESM) and regional climate models (RCM). We used the ensemble means of six
295 CORDEX projections for two Representative Concentration Pathways (RCP) scenarios: the
296 medium warming RCP4.5 and the high warming RCP8.5 scenario (for selected RCM/ESM
297 simulations see Fig. S9; https://na-cordex.org/simulations-modeling-group). We used both RCPs
298 to compare the scenario leading to the strongest warming (RCP8.5) with a more moderate
299 scenario (RCP4.5). Currently, global net CO_2 emissions follow the most pessimistic CO_2
300 emission scenario, but these may potentially be reduced depending on future climate policies
301 (Friedlingstein *et al.*, 2014a). To adjust for potential systematic differences between modeled
302 (CORDEX) and measured T_a, we debiased modeled T_a for each CORDEX projection before
303 calculating ensemble means by regressing it against measurements of daily T_a (Wilby *et al.*,
304 2004) from the nearest weather station in Fort Simpson (~50 km; 2006-2015; Environment
305 Canada, 2016; http://climate.weather.gc.ca/climate_data/). We constrained the regression to
306 periods when both CORDEX and weather station T_a > -5 °C as the root-mean-square-error
307 between modeled and measured T_a for colder periods increased by about 50 % (Fig. S5).

Results

Half-hourly landscape and wetland NEE

Between 10 June 2015 and 30 August 2016 wetlands and forests contributed equally to landscape flux footprints with 50±30 % (±95 % CI) and 47±28 %, respectively (and 3 % from the lake). About a third of the wetland contributions to the landscape flux footprints originated from the forest-to-wetland transition zones (i.e., total transition zone contributions to landscape flux footprints were 18±10 %). In contrast, transitions zones only contributed 3±3 % to the wetland flux footprints. NEE_{LAND} ranged from -7.9 μmol m^{-2} s^{-1} (1 %-ile) to 4.8 μmol m^{-2} s^{-1} (99 %-ile) whereas a smaller range from -5.2 μmol m^{-2} s^{-1} (1 %-ile) to 3.9 μmol m^{-2} s^{-1} (99 %-ile) was observed for NEE_{WET} (Fig. 2a). Positive NEE_{LAND} was more positive (i.e., more net CO_2 release) than NEE_{WET} and negative NEE_{LAND} was more negative (i.e., more net CO_2 uptake) than NEE_{WET} with a total least-squares (TLS) slope between NEE_{WET} and NEE_{LAND} of 1.49±0.03 and an intercept of 0.24±0.03 μmol m^{-2} s^{-1}. Slopes for this relationship were independent of wetland contributions (FP_{WET}; %) to landscape flux footprints. The slope for periods with FP_{WET} smaller than or equal to 50 % (1.50±0.05) was not significantly different ($\alpha = 0.05$) from the slope for periods with FP_{WET} larger than 50 % (1.43±0.03). Slopes were consistently positive for night- and daytime NEE_{LAND} against NEE_{WET} relationships. However, the nighttime slope for low FP_{WET} (1.32±0.18) was significantly smaller than the slope for high FP_{WET} (1.81±0.15), indicating that nighttime NEE_{LAND} differed more from NEE_{WET} when wetland contributions to landscape flux footprints were large. For the daytime NEE_{WET} and NEE_{LAND} relationships, the slope for high FP_{WET} of 1.52±0.05 was significantly smaller than the slope for low FP_{WET} of 1.71±0.07. NEE_{LAND} and NEE_{WET} relationships were independent of wind direction (Fig. S2) as

slopes for periods with northerly winds with overlapping wetland and landscape flux footprints were similar to slopes for periods with non-overlapping footprints (Fig. S2).

Daily landscape and wetland NEE and their component fluxes

Monthly medians of daily NEE_{LAND} and NEE_{WET} were negative from May to August (i.e., net CO_2 uptake period) when minimum daily T_a were generally warmer than 0 °C and positive for the remaining eight months with minimum daily T_a at or below 0 °C for most of the days (Fig. 3a, Fig. S3 & S4). Maximum positive daily NEE_{LAND} and NEE_{WET} were observed in November 2015 with medians of 0.48 μmol m^{-2} s^{-1} and 0.46 μmol m^{-2} s^{-1}, respectively, when T_a was below 0 °C, maximum SW_{in} smaller than 200 W m^{-2}, but soil temperatures in the wetlands (at 32 cm) still between 1 °C and 2.5 °C (Fig. S4). Minimum negative NEE_{WET} and NEE_{LAND} in 2016 occurred in July with -0.86 μmol m^{-2} s^{-1} and -1.01 μmol m^{-2} s^{-1}, respectively. From May to July 2015 monthly medians of daily NEE_{LAND} were more negative than NEE_{WET} (Wilcoxon signed-rank test; $p < 0.05$). In contrast, the median of daily NEE_{LAND} was less negative than NEE_{WET} in August 2015 (Wilcoxon signed-rank test; $p < 0.001$) and not significantly different during the same month in 2016. Monthly medians of daily NEE_{LAND} in September, October, and December were more positive than NEE_{WET} while no significant differences were observed for the remaining winter months. Differences in the derived daily component fluxes GPP and ER were more pronounced with monthly medians of daily GPP_{WET} and ER_{WET} being significantly smaller than GPP_{LAND} and ER_{LAND} from March to November (Fig. 3 b & c). During the winter months between December and April, differences in landscape and wetland GPP and ER were smaller than 0.1 μmol m^{-2} s^{-1}. The largest GPP and ER differences were observed in June 2015 with monthly medians of GPP_{WET} being 1.8 μmol m^{-2} s^{-1} smaller than medians of GPP_{LAND} and

353 monthly medians of ER_{WET} being 1.6 µmol m^{-2} s^{-1} smaller than medians of ER_{LAND}. In 2016, the
354 largest differences in monthly medians of GPP and ER were observed in July with 1.5 µmol m^{-2}
355 s^{-1} and 1.3 µmol m^{-2} s^{-1}, respectively. Between 2015 and 2016, the patterns and magnitude of
356 NEE, GPP, and ER from both towers were similar for the overlapping months April to August.
357
358 **Annual landscape and wetland NEE**
359 Annual cumulative NEE_{LAND} and NEE_{WET} (ΣNEE, g C-CO_2 m^{-2}; 1 August 2015 to 31
360 July 2016) were not significantly different with -20.1 g C-CO_2 m^{-2} (-14.6 to -26.9 g C-CO_2 m^{-2}
361 [95 % CI]) and -23.5 g C-CO_2 m^{-2} (-19.6 to -35.1 g C-CO_2 m^{-2}), respectively (Fig. 4). Both the
362 landscape and the wetland were thus small net CO_2 sinks. Shortly after snowmelt, the landscape
363 and wetland wintertime net CO_2 source switched to a net CO_2 sink. From August 2015 until the
364 end of snowmelt in 2016, ΣNEE_{LAND} was more positive (65.1 g C-CO_2 m^{-2}) than ΣNEE_{WET} (39.3
365 g C-CO_2 m^{-2}). The following larger landscape net CO_2 uptake between May and July 2016
366 reduced the annual ΣNEE differences to 3.4 g C-CO_2 m^{-2}. Only in the beginning of January,
367 wetland soil temperature (at 32 cm) dropped near the freezing temperature of water (Fig. S4) and
368 the mean early winter (October to December) respiratory net CO_2 losses at the wetland and
369 landscape tower dropped by more than 50 %, remaining low until snowmelt (January to April).
370 In contrast to ΣNEE_{LAND} and ΣNEE_{WET}, the ΣGPP_{LAND} of 532 g C-CO_2 m^{-2} was larger than the
371 ΣGPP_{WET} of 378 g C-CO_2 m^{-2}. Similarly, the ΣER_{LAND} (512 g C-CO_2 m^{-2}) exceeded the ΣER_{WET}
372 (355 g C-CO_2 m^{-2}, data not shown).
373

374 **Meteorological controls of potential NEE, GPP, and ER**

375 While both GPP_{LAND} and ER_{LAND} increased consistently with T_a, the largest mean daily
376 net CO_2 uptake (NEE_{LAND}) was observed at mean daily T_a of approximately 15 °C (Tab. 1 & Fig.
377 5). Daily mean NEE_{POT} was ~0 μmol m^{-2} s^{-1} for mean daily T_a < 2 °C, became increasingly more
378 negative at warmer T_a reaching a minimum of ~-2 μmol m^{-2} s^{-1} at about 15 °C, before it became
379 again slightly less negative for warmer T_a (Fig. 5a). Currently, mean daily T_a at Fort Simpson is
380 below 2 °C on more than 50 % of the days of the year (median of 0.2 °C; 2006-2015). In
381 contrast, only about 43 % of days are projected to be below this threshold at the end of the 21st
382 century for the RCP 8.5 scenario (median of 4.8 °C; 2091-2100). Under the current climate,
383 15 % of daily T_a exceed the optimum NEE_{POT} temperature of 15 °C. The fraction of days with
384 daily T_a above this threshold is projected to rise to 30 % (RCP8.5) by the end of the 21st century.
385 Both T_a and SW_{in} limit GPP_{POT} (Fig. 5 b - d). Maximum mean daily GPP_{LAND} of ~6 μmol m^{-2} s^{-1}
386 was observed when mean daily T_a and T_{a_week} were warmer than 15 °C and mean daily SW_{in} was
387 larger than ~200 W m^{-2}. Mean daily ER_{LAND} rapidly increased with T_a above the freezing point
388 reaching a maximum ER_{LAND} of ~5 μmol m^{-2} s^{-1} at T_a warmer than 20 °C. The T_a-based Q_{10}-
389 model explained 75 % of the variance in daily ER_{LAND} (root-mean-square error (RMSE): 0.8
390 μmol m^{-2} s^{-1}; for model parameters see Fig. 6 & Tab. S1). The combined T_a-SW_{in} model of
391 GPP_{LAND} explained 88 % of the variance in daily GPP_{LAND} (RMSE: 0.7 μmol m^{-2} s^{-1}; for model
392 parameters see Tab. S1). Modeled NEE_{MOD} - the difference between GPP_{MOD} and ER_{MOD} -
393 explained 45 % of the variance in mean daily NEE_{LAND} (RMSE: 0.7 μmol m^{-2} s^{-1}).
394

395 **Temperature- and light-limitation of GPP_{POT}**

396 During the measurement period, GPP_{POT} was mainly temperature-limited in late winter
397 (until early May) with cold T_a suppressing GPP despite high SW_{in} (Fig. 5 d & Fig. 7 a). With
398 warming T_a in June 2016, the fraction of days when GPP_{POT} was T_a-limited dropped to 33 %
399 compared to 94 % in May 2016 (Fig. 7a). In July 2016, GPP_{POT} was co-limited by T_a and SW_{in}
400 on 74 % of days (Fig. 7b). Light-limitation of GPP was rare until July ($\leq$ 10 % of days) and
401 became more frequent in August and October with 19 % and 23 % of days, respectively (Fig.
402 7c). From July to September, the fraction of days with T_a-limited GPP increased again from
403 13 % to 87 %.

404 Until the end of the 21st century (2091-2100), mean daily T_a between April and
405 September at Scotty Creek is projected to increase by 2.5 °C for the RCP 4.5 or by 5.2 °C for the
406 RCP 8.5 scenario compared to the period 2006 to 2015 (Fig. S6a-d). In contrast, mean daily
407 SW_{in} for the same period is projected to decrease by 3 W m^{-2} (RCP 4.5) and by 6.6 W m^{-2} (RCP
408 8.5), most likely due to increased cloudiness as indicated by concurrent increases in precipitation
409 (Fig. S6 e-l). These projected changes consistently reduce T_a-limitation of GPP_{POT} between April
410 and October. The largest reduction in the fraction of days with T_a-limited GPP_{POT} is expected in
411 June and September with -26 % and -22 % for the RCP 4.5 scenario and with -45 % and -47 %
412 for the RCP 8.5 scenario, respectively. The largest increase in days with co-limited GPP_{POT} is
413 projected for June (+24 % [RCP 4.5] and +40 % [RCP 8.5]). Increases in the fraction of days
414 with SW_{in}-limited GPP_{POT} are most pronounced in September with 14 % (RCP 4.5) and 37 %
415 (RCP 8.5). Between March and July, projected increases in days with SW_{in}-limited GPP_{POT} are
416 smaller than 10 % (RCP 4.5 and RCP 8.5).
417

418 **Projected changes in GPP_{MOD}, ER_{MOD}, and NEE_{MOD}**

419 By the end of the 21st century, the projected changes in T_a and SW_{in} enhance GPP_{MOD}
420 with maximum increases in May (Fig. 8). For the RCP 8.5 scenario, the projected increase in
421 annual GPP_{MOD} is about twice as large as for the RCP 4.5 scenario. However, the increase in
422 annual ER_{MOD} for the RCP 8.5 scenario is 2.5 times larger than for the RCP 4.5 scenario due to
423 warmer T_a. In contrast to GPP_{MOD}, monthly ER_{MOD} is expected to increase most strongly in
424 August and July. The differences in the timing of increases in GPP_{MOD} and ER_{MOD} result in a
425 more negative NEE_{MOD} early in the summer and less negative NEE_{MOD} in July - the warmest
426 summer month. Annual NEE_{MOD} switches its sign from -9±39 g C-CO_2 m^{-2} (±95 % CI; 2006-
427 2015) to +16±42 g C-CO_2 m^{-2} (2091-2100) for the RCP 4.5 scenario and becomes a significant
428 net CO_2 source with +94±54 g C-CO_2 m^{-2} (2091-2100) for the RCP 8.5 scenario. Similar annual
429 NEE_{MOD} for the wetland (i.e., NEE_{MOD} derived from GPP_{WET} and ER_{WET}) was modeled with
430 projected annual NEE_{MOD} (2091-2100) of -9±27 g C-CO_2 m^{-2} and +60±31 g C-CO_2 m^{-2} for the
431 RCP 4.5 and the RCP 8.5 scenario, respectively (Fig. S7). While climatic changes both in winter
432 and summer contribute to this change in annual NEE_{MOD}, the bulk of the reduction occurs during
433 the summer months (May to September) for the RCP 8.5 scenario (73 %). For the RCP 4.5
434 scenario, an equal reduction occurs during the cold (October to April) and warm season (May to
435 September).
436
437 **Discussion**
438 **Indirect thaw-induced climate change impact on carbon dioxide fluxes**
439 At Scotty Creek, both half-hourly net CO_2 uptake during the day and net CO_2 release
440 during the night were larger for the boreal forest-wetland landscape compared to the wetland
441 (Fig. 2). However, half-hourly NEE_{LAND} differed more from NEE_{WET} with increasing wetland

442 contributions to landscape flux footprints. In contrast, sensible and latent heat (Helbig *et al.*,
443 2016b) and methane fluxes (Helbig *et al.*, in press) were found to scale with wetland
444 contributions at Scotty Creek. An analysis of mean flux footprint contributions from forest-
445 wetland transition zones revealed that these contributions were about six times larger for
446 landscape than for wetland tower flux footprints (Fig. 1 c). The transition zones with higher soil
447 moisture and warmer soil temperatures (Bubier *et al.*, 1995; Baltzer *et al.*, 2014) may be
448 characterized by larger GPP and ER compared to the interior of the wetlands and the forests,
449 both characterized by drier surface soils. Such spatial patterns of GPP and ER have previously
450 been observed in similar permafrost peatlands using chamber methods (Turetsky *et al.*, 2002;
451 Wickland *et al.*, 2006; Myers-Smith *et al.*, 2007). Methane fluxes may be more uniform across
452 the wetland as these are more sensitive to variations in water table position compared to
453 variations in surface soil moisture (e.g., Bubier *et al.*, 1995; Kettunen, 2003). In contrast, the
454 productivity of the dominant plant genus in the wetland, *Sphagnum* spp., is strongly controlled
455 by surface moisture (e.g., Schipperges & Rydin, 1998), potentially explaining the differing
456 spatial patterns of NEE and methane fluxes.

457 Similar findings were reported for a thawing tundra landscape, where both GPP and ER
458 of actively thawing patches within the landscape were larger than the integrated landscape GPP
459 and ER (Belshe *et al.*, 2012). Permafrost thaw increases the availability of nitrogen (Finger *et al.*,
460 2016), increases surface soil moisture, and induces vegetation shifts toward more aquatic species
461 (Camill, 1999; Camill *et al.*, 2001), potentially enhancing both productivity and respiration in the
462 transition zones. Compared to the permafrost-free wetland, the larger extent of actively thawing
463 transition zones in the boreal forest-wetland landscape may therefore cause larger GPP_{LAND} and
464 ER_{LAND} (Fig. 2).

In contrast to ΣGPP and ΣER, annual ΣNEE_{LAND} and ΣNEE_{WET} did not differ significantly at Scotty Creek (Fig. 3), suggesting that thaw-induced wetland expansion and forest loss might have a negligible short-term impact on ΣNEE. The long-term negative ΣNEE (i.e., net CO_2 uptake) is a major component of peatland C budgets in addition to the typical C losses due to methane emissions and due to net lateral export of dissolved organic C (e.g.; Roulet *et al.*, 2007). At Scotty Creek, wetlands emit 12 g C-CH_4 m^{-2} per year as opposed to 6 g C-CH_4 m^{-2} at the landscape level (Helbig *et al.*, in press), suggesting a similar wetland and landscape net C uptake of -12 g C m^{-2} yr^{-1} (-24 g C-CO_2 m^{-2} + 12 g C-CH_4 m^{-2}) and -14 g C m^{-2} yr^{-1} (-20 g C-CO_2 m^{-2} + 6 g C-CH_4 m^{-2}), respectively (excluding lateral export of dissolved organic C [DOC]). For a boreal peatland landscape in the discontinuous permafrost zone of Manitoba, Moore (2003) reports small annual DOC exports between 1.7 and 3.2 g C m^{-2} yr^{-1}. If DOC exports at Scotty Creek are of a similar magnitude, a current net C uptake of approximately 10 g C m^{-2} yr^{-1} can be expected. A multi-site synthesis study reports similar long-term C accumulation rates for boreal permafrost peatlands [14 g C m^{-2} yr^{-1}] and for permafrost-free bogs [18 g C m^{-2} yr^{-1}] (Treat *et al.*, 2016). Similarly, growing-season NEE was not significantly different across a thaw chronosequence from a forested permafrost peat plateau to a collapse-scar bog in Alaska (Johnston *et al.*, 2014). For a permafrost peatland landscape in northern Manitoba, aboveground net primary productivity of permafrost peat plateaus and of collapse-scar bogs was similar, but a twofold increase in the accumulation of peat was observed following thaw (Camill *et al.*, 2001). Post-thaw increases in C accumulation have been reported for several thawing permafrost peatlands in Manitoba, Saskatchewan, Alberta, and Alaska (Camill, 1999; Turetsky *et al.*, 2000; Turetsky *et al.*, 2007; Jones *et al.*, 2013). However, enhanced decomposition of thawed forest peat has also been shown to exceed increased C accumulation rates in near-surface collapse-scar

488 bog peat, inducing a rapid post-thaw net C loss (O'Donnell *et al.*, 2012). Particularly transition
489 zones may be subject to rapid net C losses, before they slowly return to a net C sink after about a
490 decade (Jones *et al.*, 2016). Our findings suggest that thawing boreal forest-wetland landscapes
491 can still act as net CO_2 sinks – and most likely as net C sinks - under the current climate. The
492 continuing net CO_2 sink may be the result of integrating large areas with small net CO_2 uptake
493 (e.g., forested permafrost plateaus and interior of permafrost-free wetlands) and small areas with
494 potentially large net CO_2 loss (e.g., recently thawed transition zones). While the thaw-induced
495 wetland expansion may affect long-term C cycle dynamics through its effect on regional
496 hydrology (Connon *et al.*, 2014), species-specific productivity (Camill *et al.*, 2001), and fire
497 regimes (Camill *et al.*, 2009), the immediate indirect climate warming impact of such land cover
498 change on landscape NEE appears to be small.
499
500 **Direct climate change impacts on carbon dioxide fluxes**
501 In contrast to the small indirect thaw-induced climate change impact on NEE, direct
502 climate change effects appear to be larger and may depend strongly on the future CO_2 emission
503 trajectories as represented by RCPs (Fig. 8). At Scotty Creek, early summer NEE_{MOD} increases
504 with warming T_a, but decreases later in the summer. Such a seasonal pattern is supported by
505 multi-year observations of NEE at other northern and alpine ecosystems (Huxman *et al.*, 2003;
506 Piao *et al.*, 2008). Mid-summer GPP is often light-saturated and warmer summer T_a only
507 marginally enhances plant productivity. ER is mainly temperature-limited (in the absence of
508 moisture stress) and warmer mid-summer T_a reduces NEE by enhancing ER (Huxman *et al.*,
509 2003). In a warmer climate with more hot summer days (Fig. 5a), this increase in ER may
510 eventually exceed GPP (Runkle *et al.*, 2013). At the tree level, increased white spruce tree-ring

511 growth in Alaska has been related to warmer spring temperatures for some individuals but also to
512 decreased growth in response to warmer summer temperatures for other individuals (Wilmking
513 *et al.*, 2004). Similar to this study, recent tree-ring and modelling analyses highlight the negative
514 impacts of warmer summer T_a - and an associated increase in autotrophic respiration - on net
515 primary productivity (i.e., balance between GPP and autotrophic respiration) of black spruce
516 forests (Girardin *et al.*, 2016). Additionally, warmer summer T_a may accelerate
517 evapotranspiration rates, decrease moisture availability, and enhance atmospheric water demand
518 potentially slowing down GPP and/or ER during peak growing season (e.g.; Barber *et al.*, 2000;
519 Kljun *et al.*, 2007; Novick *et al.*, 2016).

520 In fall, light-limitation of GPP is more frequent than in spring (Niu *et al.*, 2011; Fig. 7),
521 potentially explaining the larger spring response in GPP_{MOD} to warmer T_a. For a subalpine forest,
522 Huxman *et al.* (2003) found two NEE minima in early and late summer with a reduction in net
523 CO_2 uptake in mid-summer. Here, we observed only one NEE minimum in July for the current
524 seasonal NEE pattern at Scotty Creek. However, similar to Huxman *et al.* (2003), projected
525 NEE_{MOD} is characterised by two minima in June and August for the RCP 4.5 scenario. In the
526 RCP 8.5 scenario, the NEE_{MOD} minima in early and late summer are even more pronounced (Fig.
527 8).

528 In a recent modeling synthesis study, McGuire *et al.* (2016) found that moderate warming
529 in the northern circumpolar permafrost region increased GPP, and vegetation C stocks, but
530 decreased soil C stocks over a 50-year time period in most ESMs. Atmospheric inversion models
531 indicate an increasing net CO_2 sink in the boreal biome for the period 1985 to 2012 (Welp *et al.*,
532 2016; 50° - 60° N). These results are supported by site-level NEE measurements for temperate
533 and boreal forests indicating that earlier spring onset (i.e., warmer T_a) consistently increases

GPP, and to a lesser extent ER (Kljun *et al.*, 2007; Richardson *et al.*, 2009; Richardson *et al.*, 2010). However, the positive productivity response of evergreen coniferous forests appears to be smaller compared to deciduous forests (Kljun *et al.*, 2007; Welp *et al.*, 2007; Richardson *et al.*, 2010). In a boreal forest ecosystem in the sporadic permafrost zone, longer growing seasons did not increase net CO_2 uptake as the positive productivity response was offset by enhanced respiration (Dunn *et al.*, 2007). In a boreal forest warming experiment, bud burst of black spruce trees occurred earlier and greater shoot lengths were observed (Bronson *et al.*, 2009). The increase in photosynthetic tissue may therefore enhance aboveground net primary productivity, even in the absence of changes in light-saturated photosynthesis and foliage respiration per m^2 of foliage (Bronson & Gower, 2010). Concurrent observations of decreases in fine root net primary productivity may, however, result in unchanged total net primary productivity (Bronson *et al.*, 2008).

Availability of organic C in permafrost peatland landscapes, such as Scotty Creek, is not limited (Treat *et al.*, 2016). Warmer T_a may therefore gradually increase ER while the dominant temperature-limitation of GPP may switch to a more dominant light-limitation, limiting the productivity benefits of warming T_a (Fig. 6 and 7). Air temperature effects on ER have been shown to exert a strong control on interannual variation of boreal forest NEE, exceeding the impacts of variations in GPP (Ueyama *et al.*, 2009; Ueyama *et al.*, 2014). In boreal forests, the NEE response to T_a often follows a parabolic curve with a temperature-optimum of NEE followed by decreasing net CO_2 uptake with T_a above this threshold (Grant *et al.*, 2009; Niu *et al.*, 2011; Fig. 6a). At Scotty Creek, this T_a-threshold appears to be approximately 15 °C, slightly warmer than the 11-year mean NEE T_a-optimum of 11±2 °C (± one standard deviation) for a boreal forest in the sporadic permafrost zone of northern Manitoba (Niu *et al.*, 2012). It should

be noted that, in the long-term, the NEE temperature-optimum might change with thermal adaptation of the vegetation or species composition shifts (Yuan *et al.*, 2011). In a warmer climate, the T_a-optimum of NEE in boreal landscapes like Scotty Creek is likely to be exceeded more often during the summer (Fig. 5a), potentially decreasing summertime net CO_2 uptake. Our results suggest that, with continuously rising T_a, increases in net CO_2 uptake of boreal forest-wetland landscapes may therefore eventually slow down, and their long-term net CO_2 uptake may potentially decrease depending on the climate-warming scenario.

A decreasing potential of boreal forest-wetland landscapes to sequester CO_2 in a warmer climate is supported by a projected C loss at the southern edge of the boreal biome where ecosystems with low potential for long-term C accumulation are expected to replace current boreal organic C-rich ecosystems (Koven, 2013). A diminishing potential net CO_2 uptake may "push" the current C-accumulating landscapes to an unstable state increasing the potential for an abrupt transition to landscapes with lower C stocks and a loss of their CO_2 sink function (Scheffer *et al.*, 2012). For the RCP4.5 scenario, current climates (i.e., mean annual T_a and total precipitation) similar to the projected end-of-the-century climate of Scotty Creek are found within the boreal biome in northern Alberta. For the RCP8.5 scenario, similar climates are currently found at the limit or south of the boreal biome in Canada and the northwestern United States (Fig. 9 and Fig. S8). In contrast to changes in T_a and precipitation, SW_{in} is more strongly bound to latitude. The limited duration of the period providing sufficient light for photosynthetic CO_2 uptake combined with warmer T_a and more precipitation (Fig. S6) is therefore likely to increase ER more than GPP, particularly for the RCP8.5 scenario (Fig. 8). A shift from permafrost peatland landscapes with large organic C stocks (mean of 106 kg m^{-2} ± 45 [± one standard deviation] for forested permafrost plateaus [n = 158]; 117 kg m^{-2} ± 65 for collapse-scar

580 bogs [n = 52]; data from Treat *et al.*, 2016) to landscapes with low C stocks would result in large
581 net CO_2 emissions. Our results suggest that the magnitude of these emissions will strongly
582 depend on future anthropogenic CO_2 emission pathways (Fig. 8).
583
584 **Comparison with Earth system models and CO_2 flux inversion modeling**
585 A comparison with five end-of-21st-century ESM projections of NEE (from the Coupled
586 Model Intercomparison Project [CMIP5; http://cmip-pcmdi.llnl.gov/cmip5/]; Friedlingstein *et*
587 *al.*, 2014b; Fig. S9) shows that three out of five ESMs project NEE changes similar to our
588 findings. More specifically, for the southern Taiga Plains region, no ESM shows significant
589 changes in mean annual NEE for the moderate RCP4.5 scenario (Two-Sample t-test; $\alpha = 0.05$; n
590 = 10). For the warmer RCP8.5 scenario, three out of the five ESMs indicate decreases in net CO_2
591 uptake (7 to 36 g C-CO_2 m^{-2} less negative NEE with one ESM showing a significant decrease; p
592 = 0.04; n = 10; see Fig. S9). Two ESMs even indicate a switch from a net CO_2 sink to a net CO_2
593 source. Similar to our study, all ESMs project the largest monthly increase in net CO_2 uptake
594 between April and June (except for July in the RCP8.5 scenario of one ESM) and smaller
595 increases or even decreases in net CO_2 uptake later in summer.
596 For the period 2006 to 2015, all five ESMs indicate a mean net CO_2 sink for the southern
597 Taiga Plains region with differences of less than 20 g C-CO_2 m^{-2} to measured annual NEE at
598 Scotty Creek (except for a larger difference for one ESM; Fig. S10). Compared to the annual
599 landscape NEE of -20 g C-CO_2 m^{-2} at Scotty Creek, global CO_2 flux inversions (1° x 1°
600 resolution, CarbonTracker, 2016) suggest a mean annual NEE (2006 – 2015) of -39±52 g C-CO_2
601 m^{-2} [± one standard deviation] with a similar monthly NEE seasonality and magnitude (Fig.
602 S10a). However, four out of five ESMs overestimate the maximum monthly net CO_2 uptake in

603 the summer and the maximum monthly net CO_2 loss in the winter. The ESMs simulate both
604 direct and indirect climate change effects on NEE, but their NEE response may vary due to
605 differing representations of land surface processes (e.g., dynamic vegetation models, phenology,
606 CO_2 fertilization, nutrient dynamics) (e.g., Friedlingstein *et al.*, 2014b; Wieder *et al.*, 2015).
607 Disentangling the individual contributions from these processes to diverging NEE projections is
608 difficult due to the complex interactions between the individual model components (e.g.,
609 Friedlingstein *et al.*, 2014b). However, an improved understanding of temperature- and light-
610 limitation of NEE may help reducing the wide spread in modeled boreal landscape NEE response
611 to climate change and minimize the deviation between measured and modeled seasonality of
612 NEE.
613
614 **Potential responses of ecosystem functioning to a changing climate**
615 How vegetation productivity and respiration respond to changes in temperature and light
616 may be affected by factors other than shifts in landscape and ecosystem composition and
617 structure. Rising atmospheric CO_2 concentrations and the related fertilization effect on plant
618 productivity may stimulate and enhance GPP (McGuire *et al.*, 2016). This CO_2 fertilization
619 effect could directly increase GPP through its positive impact on maximum GPP (Ueyama *et al.*,
620 2016), favoring a larger potential for net CO_2 uptake than projected in this study. However, the
621 magnitude of the CO_2 fertilization effect in boreal forests remains poorly constrained: both no
622 productivity response (Kroner & Way, 2016) and a positive response was observed (Tjoelker *et*
623 *al.*, 1998) in CO_2 fertilization experiments of Norway spruce (*Picea abies*) and black spruce
624 seedlings. A small, positive GPP response of 0.16 % ppm^{-1} (2002-2014) was estimated for an
625 Alaskan black spruce forest (Ueyama *et al.*, 2016). Net primary productivity of about half of the

626 black spruce forests in North America (south of 60° N) was projected to decline at the end of the
627 21st century in a modeling study despite a positive CO_2 fertilization effect on GPP (Girardin *et*
628 *al.*, 2016). For *Sphagnum* spp. and vascular bog species, only small or negative CO_2 effects on
629 productivity were reported (Berendse *et al.*, 2001; Heijmans *et al.*, 2002). To some extent, plants
630 can acclimate to warmer T_a by modifying their photosynthetic and respiratory apparatus. In
631 warming and CO_2 enrichment experiments, the thermal optimum of light-saturated net CO_2
632 uptake of both Norway spruce and black spruce seedlings increased in the warming treatments
633 while leaf respiration was suppressed. At the same time, light-saturated net CO_2 uptake was
634 found to decrease for the warmest treatments (+8 °C) (Way & Sage, 2008; Kroner & Way,
635 2016). A better constraint of the impacts of CO_2 fertilization and thermal acclimation on the
636 productivity of boreal plant species is therefore needed to fully understand the response of boreal
637 forest-wetland landscape CO_2 fluxes to climate change.

638 Our focus on meteorological controls (temperature and light) of GPP only constrains the
639 GPP_{MOD} response given no other limiting factors. Actual GPP however may be reduced by
640 additional environmental limitations. For example, earlier spring onset in the boreal and
641 temperate forests has been observed to decrease peak summer productivity due to soil moisture
642 deficits later in the summer (Buermann *et al.*, 2013; Wolf *et al.*, 2016). Particularly in late
643 summer and fall, soil moisture deficits can add another environmental constraint on GPP (Niu *et*
644 *al.*, 2011). In peatlands, fluctuating water levels may also modify the temperature-sensitivity of
645 heterotrophic soil respiration (e.g., Silvola *et al.*, 1996; Hanis *et al.*, 2015) and affect GPP (e.g.,
646 Chivers *et al.*, 2009). Changes in net primary productivity may alter C substrate availability to
647 soil microbes through changes in litter fall (Bond-Lamberty *et al.*, 2004; Beier *et al.*, 2008) and
648 changes in GPP may affect autotrophic respiration through the allocation of photosynthates

649 (Janssens *et al.*, 2001). Such indirect effects of ecosystem acclimation may modify the overall
650 temperature sensitivity of ER and, therefore, additionally affect NEE responses to a changing
651 climate. The temperature-response of ER in a warmer climate could also be attenuated if
652 increasing net C losses diminish the fraction of labile organic C, exposing more recalcitrant
653 organic matter from deeper peat layers, or induce temperature-related changes in soil microbial
654 communities (Hogg *et al.*, 1992; Bradford *et al.*, 2008). Understanding how these environmental
655 controls interact with the warming-related shifts in the seasonality of GPP and ER will help
656 constraining the NEE response to a warmer climate.

657 Here, we show that thaw-induced wetland expansion and associated boreal forest loss
658 appears to have negligible indirect climate change effects on the observed landscape net CO_2
659 uptake of ~20 g C-CO_2 m^{-2} yr^{-1}. However, even without moisture stress, net CO_2 uptake of
660 boreal forest-wetland landscapes is likely to decline by the end of the 21st century due to direct
661 climate change impacts of changing meteorological forcing. This projected reduction is about
662 five times larger for a high climate-warming scenario (103 g C-CO_2 m^{-2} yr^{-1}) compared to a
663 moderate scenario (25 g C-CO_2 m^{-2} yr^{-1}). In an exceedingly warmer climate, the recently
664 observed increasing net CO_2 uptake of the boreal biome may therefore turn into a decreasing net
665 CO_2 sink during the 21st century, reducing the ability of boreal landscapes to sequester
666 atmospheric CO_2.

Acknowledgements

We thank three anonymous reviewers for their critical and constructive comments. MH was funded through graduate student scholarships provided by the Fonds de recherche du Québec – Nature et technologies (FRQNT) and the German Academic Exchange Service (DAAD). Funding for this research was awarded to OS by the Canada Research Chairs, Canada Foundation for Innovation Leaders Opportunity Fund and Natural Sciences and Engineering Research Council Discovery Grant programs. ARD acknowledges support from the U.S. Dept of Energy Lawrence Berkeley Lab Ameriflux Network Management Project. MH is thankful to Tanja Živković, Avni Malhotra, and Christoforos Pappas for discussions improving an earlier version of the manuscript. We are grateful for the support of the Liidlii Kue First Nation and Jean-Marie River First Nation for their support of the Scotty Creek Research Station. This study was part of the Arctic Boreal Vulnerability Experiment (ABoVE).

References

Baltzer JL, Veness T, Chasmer LE, Sniderhan AE, Quinton WL (2014) Forests on thawing permafrost: fragmentation, edge effects, and net forest loss. *Global Change Biology*, **20**, 824–834.

Barber VA, Juday GP, Finney BP (2000) Reduced growth of Alaskan white spruce in the twentieth century from temperature-induced drought stress. *Nature*, **405**, 668–673.

Beier C, Emmett BA, Peñuelas J et al. (2008) Carbon and nitrogen cycles in European ecosystems respond differently to global warming. *Science of the Total Environment*, **407**, 692–697.

Belshe EF, Schuur EAG, Bolker BM, Bracho R (2012) Incorporating spatial heterogeneity created by permafrost thaw into a landscape carbon estimate. *Journal of Geophysical Research: Biogeosciences*, **117**, G01026.

Berendse F, Van Breemen N, Rydin Ha et al. (2001) Raised atmospheric CO_2 levels and increased N deposition cause shifts in plant species composition and production in Sphagnum bogs. *Global Change Biology*, **7**, 591–598.

Bond-Lamberty B, Wang C, Gower ST (2004) A global relationship between the heterotrophic and autotrophic components of soil respiration? *Global Change Biology*, **10**, 1756–1766.

Bradford MA, Davies CA, Frey SD et al. (2008) Thermal adaptation of soil microbial respiration to elevated temperature. *Ecology Letters*, **11**, 1316–1327.

Brandt JP (2009) The extent of the North American boreal zone. *Environmental Reviews*, **17**, 101–161.

Bronson DR, Gower ST (2010) Ecosystem warming does not affect photosynthesis or aboveground autotrophic respiration for boreal black spruce. *Tree Physiology*, **30**, 441–449.

Bronson D, Gower ST, Tanner M, Linder S, Van Herk I (2008) Response of soil surface CO_2 flux in a boreal forest to ecosystem warming. *Global Change Biology*, **14**, 856–867.

Bronson DR, Gower ST, Tanner M, Van Herk I (2009) Effect of ecosystem warming on boreal black spruce bud burst and shoot growth. *Global Change Biology*, **15**, 1534–1543.

Bubier JL (1995) The relationship of vegetation to methane emission and hydrochemical gradients in northern peatlands. *Journal of Ecology*, **83**, 403–420.

Bubier JL, Moore TR, Bellisario L, Comer NT, Crill M (1995) Ecological controls on methane emissions from a northern peatland complex in the zone of discontinuous permafrost, Manitoba, Canada. *Global Biogeochemical Cycles*, **9**, 455–470.

Buermann W, Bikash PR, Jung M, Burn DH, Reichstein M (2013) Earlier springs decrease peak summer productivity in North American boreal forests. *Environmental Research Letters*, **8**, 24027.

Camill P (1999) Peat accumulation and succession following permafrost thaw in the boreal peatlands of Manitoba, Canada. *Écoscience*, **6**, 592–602.

Camill P, Lynch JA, Clark JS, Adams JB, Jordan B (2001) Changes in biomass, aboveground net primary production, and peat accumulation following permafrost thaw in the boreal peatlands of Manitoba, Canada. *Ecosystems*, **4**, 461–478.

720 Camill P, Barry A, Williams E, Andreassi C, Limmer J, Solick D (2009) Climate-vegetation-fire
721 interactions and their impact on long-term carbon dynamics in a boreal peatland landscape
722 in northern Manitoba, Canada. *Journal of Geophysical Research*, **114**, G04017.

723 Chapin FS, McGuire AD, Randerson J et al. (2000) Arctic and boreal ecosystems of western
724 North America as components of the climate system. *Global Change Biology*, **6**, 211–223.

725 Chasmer LE, Hopkinson C, Quinton W (2010) Quantifying errors in discontinuous permafrost
726 plateau change from optical data, Northwest Territories, Canada: 1947-2008. *Canadian*
727 *Journal of Remote Sensing*, **36**, S211–S223.

728 Chasmer LE, Hopkinson C, Veness T, Quinton W, Baltzer J (2014) A decision-tree classification
729 for low-lying complex land cover types within the zone of discontinuous permafrost.
730 *Remote Sensing of Environment*, **143**, 73–84.

731 Chasmer LE, Hopkinson C (in press) Threshold Loss of Discontinuous Permafrost and
732 Landscape Evolution. *Global Change Biology*, doi: 10.1111/gcb.13537.

733 Chivers MR, Turetsky MR, Waddington JM, Harden JW, McGuire AD (2009) Effects of
734 experimental water table and temperature manipulations on ecosystem CO2 fluxes in an
735 Alaskan rich fen. *Ecosystems*, **12**, 1329–1342.

736 Connon RF, Quinton WL, Craig JR, Hayashi M (2014) Changing hydrologic connectivity due to
737 permafrost thaw in the lower Liard River valley, NWT, Canada. *Hydrological Processes*,
738 **28**, 4163–4178.

739 DeBeer CM, Wheater HS, Carey SK, Chun KP (2016) Recent climatic, cryospheric, and
740 hydrological changes over the interior of western Canada: a synthesis and review.
741 *Hydrology and Earth System Sciences*, **20**, 1573–1598.

742 Dunn AL, Barford CC, Wofsy SC, Goulden ML, Daube BC (2007) A long-term record of carbon
743 exchange in a boreal black spruce forest: means, responses to interannual variability, and
744 decadal trends. *Global Change Biology*, **13**, 577–590.

745 Environment Canada (2014) Canadian Climate Normals: 1981 - 2010. Available at:
746 http://climate.weather.gc.ca/climate_normals/index_e.html (accessed 15 September 2016).

747 Fang C, Moncrieff JB (2001) The dependence of soil CO_2 efflux on temperature. *Soil Biology*
748 *and Biochemistry*, **33**, 155–165.

749 Finger RA, Turetsky MR, Kielland K, Ruess RW, Mack MC, Euskirchen ES (2016) Effects of
750 permafrost thaw on nitrogen availability and plant-soil interactions in a boreal Alaskan
751 lowland. *Journal of Ecology*, **194**, 1542–1554.

752 Friedlingstein P, Andrew RM, Rogelj J et al. (2014a) Persistent growth of CO_2 emissions and
753 implications for reaching climate targets. *Nature Geoscience*, **7**, 709–715.

754 Friedlingstein P, Meinshausen M, Arora VK, Jones CD, Anav A, Liddicoat SK, Knutti R
755 (2014b) Uncertainties in CMIP5 climate projections due to carbon cycle feedbacks. *Journal*
756 *of Climate*, **27**, 511–526.

757 Frolking S, Roulet N, Fuglestvedt J (2006) How northern peatlands influence the Earth's
758 radiative budget: Sustained methane emission versus sustained carbon sequestration.
759 *Journal of Geophysical Research*, **111**, G01008.

760 Garon-Labrecque M-E, Léveillé-Bourret É, Higgins K, Sonnentag O (2015) Additions to the

761 Boreal Flora of the Northwest Territories with a Preliminary Vascular Flora of Scotty
762 Creek. *Canadian Field-Naturalist*, **129**, 349–367.

763 Gea-Izquierdo G, Makela A, Margolis HA et al. (2010) Modeling acclimation of photosynthesis
764 to temperature in evergreen conifer forests. *New Phytologist*, **188**, 175–186.

765 Girardin MP, Hogg EH, Bernier PY, Kurz WA, Guo XJ, Cyr G (2016) Negative impacts of high
766 temperatures on growth of black spruce forests intensify with the anticipated climate
767 warming. *Global Change Biology*, **22**, 627–643.

768 Grant RF, Margolis HA, Barr AG, Black TA, Dunn AL, Bernier PY, Bergeron O (2009)
769 Changes in net ecosystem productivity of boreal black spruce stands in response to changes
770 in temperature at diurnal and seasonal time scales. *Tree Physiology*, **29**, 1–17.

771 Hadden D, Grelle A (2016) Changing temperature response of respiration turns boreal forest
772 from carbon sink into carbon source. *Agricultural and Forest Meteorology*, **223**, 30–38.

773 Hanis KL, Amiro BD, Tenuta M et al. (2015) Carbon exchange over four growing seasons for a
774 subarctic sedge fen in northern Manitoba, Canada. *Arctic Science*, **1**, 27–44.

775 Heijmans MMPD, Klees H, De Visser W, Berendse F (2002) Response of a Sphagnum bog plant
776 community to elevated C02 and N supply. *Plant Ecology*, **162**, 123–134.

777 Helbig M, Chasmer LE, Kljun N, Quinton WL, Treat CC, Sonnentag O (in press) The positive
778 net radiative forcing of increasing methane emissions from a thawing boreal forest-wetland
779 landscape. *Global Change Biology*, doi: 10.1111/gcb.13520.

780 Helbig M, Pappas C, Sonnentag O (2016a) Permafrost thaw and wildfire: equally important
781 drivers of boreal tree cover changes in the Taiga Plains, Canada. *Geophysical Research*
782 *Letters*, **43**, 1598–1606.

783 Helbig M, Wischnewski K, Kljun N, Chasmer LE, Quinton WL, Detto M, Sonnentag O (2016b)
784 Regional atmospheric cooling and wetting effect of permafrost thaw-induced boreal forest
785 loss. *Global Change Biology*, doi: 10.1111/gcb.13348.

786 Helbig M, Wischnewski K, Gosselin GH et al. (2016c) Addressing a systematic bias in carbon
787 dioxide flux measurements with the EC150 and the IRGASON open-path gas analyzers.
788 *Agricultural and Forest Meteorology*, **228–229**, 349–359.

789 Hogg EH, Lieffers VJ, Wein RW (1992) Potential carbon losses from peat profiles: effects of
790 temperature, drought cycles, and fire. *Ecological Applications*, **2**, 298–306.

791 Hugelius G, Bockheim JG, Camill P et al. (2013) A new data set for estimating organic carbon
792 storage to 3 m depth in soils of the northern circumpolar permafrost region. *Earth System*
793 *Science Data*, **5**, 393–402.

794 Huxman TE, Turnipseed AA, Sparks JP, Harley PC, Monson RK (2003) Temperature as a
795 control over ecosystem CO_2 fluxes in a high-elevation, subalpine forest. *Oecologia*, **134**,
796 537–546.

797 Janssens IA, Lankreijer H, Matteucci G et al. (2001) Productivity overshadows temperature in
798 determining soil and ecosystem respiration across European forests. *Global Change*
799 *Biology*, **7**, 269–278.

800 Johnston CE, Ewing SA, Harden JW et al. (2014) Effect of permafrost thaw on CO_2 and CH_4
801 exchange in a western Alaska peatland chronosequence. *Environmental Research Letters*, **9**,

802 85004.

803 Jones MC, Booth RK, Yu Z, Ferry P (2013) A 2200-year record of permafrost dynamics and
804 carbon cycling in a collapse-scar bog, interior Alaska. *Ecosystems*, **16**, 1–19.

805 Jones MC, Harden J, O'Donnell J, Manies K, Jorgenson T, Treat C, Ewing S (2016) Rapid
806 carbon loss and slow recovery following permafrost thaw in boreal peatlands. *Global*
807 *Change Biology*, doi:10.1111/gcb.13403.

808 Kettunen A (2003) Connecting methane fluxes to vegetation cover and water table fluctuations at
809 microsite level: A modeling study. *Global Biogeochemical Cycles*, **17**, 1051.

810 Keuper F, van Bodegom PM, Dorrepaal E, Weedon JT, van Hal J, van Logtestijn RSP, Aerts R
811 (2012) A frozen feast: thawing permafrost increases plant-available nitrogen in subarctic
812 peatlands. *Global Change Biology*, **18**, 1998–2007.

813 Kirtman B, Power SB, Adedoyin JA et al. (2013) Near-term Climate Change: Projections and
814 Predictability. In: *Climate Change 2013: The Physical Science Basis. Contribution of*
815 *Working Group I to the Fifth Assessment Report of the Intergovernmental Panel on Climate*
816 *Change* (eds Stocker TF, Qin D, Plattner G-K, Tignor M, Allen SK, Boschung J, Nauels A,
817 Xia Y, Bex V, Midgley PM), pp. 953–1028. Cambridge University Press, Cambridge,
818 United Kingdom and New York, NY, USA.

819 Kljun N, Black TA, Griffis TJ et al. (2007) Response of net ecosystem productivity of three
820 boreal forest stands to drought. *Ecosystems* **10**, 1039-1055.

821 Kljun N, Calanca P, Rotach MW, Schmid HP (2015) A simple two-dimensional parameterisation
822 for Flux Footprint Predictions (FFP). *Geoscientific Model Development*, **8**, 3695–3713.

823 Knoblauch C, Beer C, Sosnin A, Wagner D, Pfeiffer E-M (2013) Predicting long-term carbon
824 mineralization and trace gas production from thawing permafrost of Northeast Siberia.
825 *Global Change Biology*, **19**, 1160–1172.

826 Koven CD (2013) Boreal carbon loss due to poleward shift in low-carbon ecosystems. *Nature*
827 *Geoscience*, **6**, 452–456.

828 Koven CD, Schuur EAG, Schädel C et al. (2015) A simplified, data-constrained approach to
829 estimate the permafrost carbon – climate feedback. *Philosophical Transactions of the Royal*
830 *Society A*, **373**, 20140423.

831 Kroner Y, Way DA (2016) Carbon fluxes acclimate more strongly to elevated growth
832 temperatures than to elevated CO_2 concentrations in a northern conifer. *Global Change*
833 *Biology*, **22**, 2913–2928.

834 Kurylyk BL, Hayashi M, Quinton WL, McKenzie JC, Voss CI (2016) Influence of vertical and
835 lateral heat transfer on permafrost thaw, peatland landscape transition, and groundwater
836 flow. *Water Resources Research*, **52**, 1286–1305.

837 Lafleur PM, Moore TR, Roulet NT, Frolking S (2005) Ecosystem respiration in a cool temperate
838 bog depends on peat temperature but not water table. *Ecosystems*, **8**, 619–629.

839 Lara MJ, Genet H, McGuire AD et al. (2016) Thermokarst rates intensify due to climate change
840 and forest fragmentation in an Alaskan boreal forest lowland. *Global Change Biology*, **22**,
841 816–829.

842 Lasslop G, Reichstein M, Papale D et al. (2010) Separation of net ecosystem exchange into

assimilation and respiration using a light response curve approach: critical issues and global evaluation. *Global Change Biology*, **16**, 187–208.

Le Quéré C, Moriarty R, Andrew RM et al. (2015) Global Carbon Budget 2015. *Earth System Science Data*, **7**, 349–396.

Luyssaert S, Inglima I, Jung M et al. (2007) CO_2 balance of boreal, temperate, and tropical forests derived from a global database. *Global Change Biology*, **13**, 2509–2537.

Mahecha MD, Reichstein M, Carvalhais N et al. (2010) Global convergence in the temperature sensitivity of respiration at ecosystem level. *Science*, **329**, 838–840.

McGuire AD, Koven CD, Lawrence DM et al. (2016) Variability in the sensitivity among model simulations of permafrost and carbon dynamics in the permafrost region between 1960 and 2009. *Global Biogeochemical Cycles*, **30**, 1015–1037.

Moore TR (2003) Dissolved organic carbon in a northern boreal landscape. *Global Biogeochemical Cycles*, **17**, 1109.

Myers-Smith IH, McGuire AD, Harden JW, Chapin FS (2007) Influence of disturbance on carbon exchange in a permafrost collapse and adjacent burned forest. *Journal of Geophysical Research*, **112**, G04017.

Natali SM, Schuur EAG, Webb EE, Hicks Pries CE, Crummer KG (2014) Permafrost degradation stimulates carbon loss from experimentally warmed tundra. *Ecology*, **95**, 602–608.

Novick KA, Ficklin DL, Stoy PC et al. (2016) The increasing importance of atmospheric demand for ecosystem water and carbon fluxes. *Nature Climate Change*, **6**, 1023–1027.

Niu S, Luo Y, Fei S et al. (2011) Seasonal hysteresis of net ecosystem exchange in response to temperature change: patterns and causes. *Global Change Biology*, **17**, 3102–3114.

Niu S, Luo Y, Fei S et al. (2012) Thermal optimality of net ecosystem exchange of carbon dioxide and underlying mechanisms. *The New Phytologist*, **194**, 775–783.

O'Donnell JA, Jorgenson MT, Harden JW, McGuire AD, Kanevskiy MZ, Wickland KP (2012) The Effects of Permafrost Thaw on Soil Hydrologic, Thermal, and Carbon Dynamics in an Alaskan Peatland. *Ecosystems*, **15**, 213–229.

Olefeldt D, Goswami S, Grosse G et al. (2016) Circumpolar distribution and carbon storage of thermokarst landscapes. *Nature Communications*, **7**, 13043.

Osterkamp TE, Viereck L, Shur Y, Jorgenson MT, Racine CH, Doyle A, Boone RD (2000) Observations of Thermokarst and Its Impact on Boreal Forests in Alaska, U.S.A. *Arctic, Antarctic, and Alpine Research*, **32**, 303–315.

Pan Y, Birdsey RA, Fang J et al. (2011) A Large and Persistent Carbon Sink in the World's Forests. *Science*, **333**, 988–994.

Papale D, Reichstein M, Aubinet M et al. (2006) Towards a standardized processing of Net Ecosystem Exchange measured with eddy covariance technique: algorithms and uncertainty estimation. *Biogeosciences*, **3**, 571–583.

Peichl M, Sonnentag O, Wohlfahrt G et al. (2013) Convergence of potential net ecosystem production among contrasting C3 grasslands. *Ecology Letters*, **16**, 502–512.

Pelletier N, Talbot J, Olefeldt D, Turetsky MR, Blodau C, Sonnentag O, Quinton WL (in press) Influence of Holocene permafrost aggradation and thaw on the paleoecology and carbon storage of a peatland complex in northwestern Canada. *The Holocene*.

Piao S, Ciais P, Friedlingstein P et al. (2008) Net carbon dioxide losses of northern ecosystems in response to autumn warming. *Nature*, **451**, 49–52.

Quinton WL, Hayashi M, Chasmer LE (2011) Permafrost-thaw-induced land-cover change in the Canadian subarctic: implications for water resources. *Hydrological Processes*, **25**, 152–158.

Rayment MB, Loustau D, Jarvis PJ (2002) Photosynthesis and respiration of black spruce at three organizational scales: shoot, branch and canopy. *Tree Physiology*, **22**, 219–29.

Reichstein M, Falge E, Baldocchi D et al. (2005) On the separation of net ecosystem exchange into assimilation and ecosystem respiration: review and improved algorithm. *Global Change Biology*, **11**, 1424–1439.

Richardson AD, Hollinger DY, Dail DB, Lee JT, Munger JW, O'Keefe J (2009) Influence of spring phenology on seasonal and annual carbon balance in two contrasting New England forests. *Tree Physiology*, **29**, 321–331.

Richardson AD, Black TA, Ciais P et al. (2010) Influence of spring and autumn phenological transitions on forest ecosystem productivity. *Philosophical Transactions of the Royal Society B: Biological Sciences*, **365**, 3227–3246.

Robinson D, Moore TR (1999) Carbon and peat accumulation over the past 1200 years in a landscape with discontinuous permafrost, northwestern Canada. *Global Biogeochemical Cycles*, **13**, 591–601.

Roulet NT, Lafleur PM, Richard PJH, Moore TR, Humphreys ER, Bubier J (2007) Contemporary carbon balance and late Holocene carbon accumulation in a northern peatland. *Global Change Biology*, **13**, 397–411.

Runkle BRK, Sachs T, Wille C, Pfeiffer E-M, Kutzbach L (2013) Bulk partitioning the growing season net ecosystem exchange of CO_2 in Siberian tundra reveals the seasonality of its carbon sequestration strength. *Biogeosciences*, **10**, 1337–1349.

Scheffer M, Hirota M, Holmgren M, Van Nes EH, Chapin FS (2012) Thresholds for boreal biome transitions. *Proceedings of the National Academy of Sciences of the United States of America*, **109**, 21384–9.

Schipperges B, Rydin H (1998) Response of photosynthesis of Sphagnum species from contrasting microhabitats to tissue water content and repeated desiccation. *New Phytologist*, **140**, 677–684.

Schuur EAG, McGuire AD, Schädel C et al. (2015) Climate change and the permafrost carbon feedback. *Nature*, **520**, 171–179.

Schuur EAG, Vogel JG, Crummer KG, Lee H, Sickman JO, Osterkamp TE (2009) The effect of permafrost thaw on old carbon release and net carbon exchange from tundra. *Nature*, **459**, 556–559.

Silvola J, Alm J, Ahlholm U, Nykanen H, Martikainen PJ (1996) CO_2 fluxes from peat in boreal mires under varying temperature and moisture conditions. *Journal of Ecology*, **84**, 219–228.

Tanja S, Berninger F, Vesala T et al. (2003) Air temperature triggers the recovery of evergreen

boreal forest photosynthesis in spring. *Global Change Biology*, **9**, 1410–1426.

Tarnocai C, Canadell JG, Schuur EAG, Kuhry P, Mazhitova G, Zimov S (2009) Soil organic carbon pools in the northern circumpolar permafrost region. *Global Biogeochemical Cycles*, **23**, GB2023.

Tjoelker MG, Oleksyn J, Reich PB (1998) Seedlings of five boreal tree species differ in acclimation of net photosynthesis to elevated CO_2 and temperature. *Tree Physiology*, **18**, 715–726.

Treat CC, Wollheim WM, Varner RK, Grandy AS, Talbot J, Frolking S (2014) Temperature and peat type control CO_2 and CH_4 production in Alaskan permafrost peats. *Global Change Biology*, **20**, 2674–2686.

Treat CC, Jones MC, Camill P et al. (2016) Effects of permafrost aggradation on peat properties as determined from a pan-Arctic synthesis of plant macrofossils. *Journal of Geophysical Research: Biogeosciences*, **121**, 78–94.

Turetsky MR, Wieder RK, Williams CJ, Vitt DH (2000) Organic matter accumulation, peat chemistry, and permafrost melting in peatlands of boreal Alberta. *Écoscience*, **7**, 379–392.

Turetsky M, Wieder K, Halsey L, Vitt DH (2002) Current disturbance and the diminishing peatland carbon sink. *Geophysical Research Letters*, **29**, 1526.

Turetsky MR, Wieder RK, Vitt DH, Evans RJ, Scott KD (2007) The disappearance of relict permafrost in boreal north America: Effects on peatland carbon storage and fluxes. *Global Change Biology*, **13**, 1922–1934.

Ueyama M, Harazono Y, Kim Y, Tanaka N (2009) Response of the carbon cycle in sub-arctic black spruce forests to climate change: Reduction of a carbon sink related to the sensitivity of heterotrophic respiration. *Agricultural and Forest Meteorology*, **149**, 582–602.

Ueyama M, Iwata H, Harazono Y (2014) Autumn warming reduces the CO_2 sink of a black spruce forest in interior Alaska based on a nine-year eddy covariance measurement. *Global Change Biology*, **20**, 1161–1173.

Ueyama M, Tahara N, Iwata H et al. (2016) Optimization of a biochemical model with eddy covariance measurements in black spruce forests of Alaska for estimating CO_2 fertilization effects. *Agricultural and Forest Meteorology*, **222**, 98–111.

Way DA, Sage RF (2008) Elevated growth temperatures reduce the carbon gain of black spruce [Picea mariana (Mill.) B.S.P.]. *Global Change Biology*, **14**, 624–636.

Wehr R, Munger JW, McManus JB et al. (2016) Seasonality of temperate forest photosynthesis and daytime respiration. *Nature*, **534**, 680–683.

Welp LR, Randerson JT, Liu HP (2007) The sensitivity of carbon fluxes to spring warming and summer drought depends on plant functional type in boreal forest ecosystems. *Agricultural and Forest Meteorology*, **147**, 172–185.

Welp LR, Patra PK, Rodenbeck C, Nemani R, Bi J, Piper SC, Keeling RF (2016) Increasing summer net CO_2 uptake in high northern ecosystems inferred from atmospheric inversions and comparisons to remote sensing NDVI. *Atmospheric Chemistry and Physics*, **16**, 9047–9066.

Wickland KP, Striegl RG, Neff JC, Sachs T (2006) Effects of permafrost melting on CO_2 and

965 CH_4 exchange of a poorly drained black spruce lowland. *Journal of Geophysical Research*,
966 **111**, G02011.

967 Wieder WR, Cleveland CC, Smith WK, Todd-Brown K (2015) Future productivity and carbon
968 storage limited by terrestrial nutrient availability. *Nature Geoscience*, **8**, 441-U35.

969 Wilby RL, Charles SP, Zorita E, Timbal B, Whetton P, Mearns LO (2004) Guidelines for Use of
970 Climate Scenarios Developed from Statistical Downscaling Methods. Available at :
971 https://www.narccap.ucar.edu/doc/tgica-guidance-2004.pdf (accessed 15 September 2016).

972 Wilmking M, Juday GP, Barber VA, Zald HSJ (2004) Recent climate warming forces
973 contrasting growth responses of white spruce at treeline in Alaska through temperature
974 thresholds. *Global Change Biology*, **10**, 1724–1736.

975 Wolf S, Keenan TF, Fisher JB et al. (2016) Warm spring reduced carbon cycle impact of the
976 2012 US summer drought. *Proceedings of the National Academy of Science*, **113**, 5880–
977 5885.

978 Yu Z (2006) Holocene Carbon Accumulation of Fen Peatlands in Boreal Western Canada: A
979 Complex Ecosystem Response to Climate Variation and Disturbance. *Ecosystems*, **9**, 1278–
980 1288.

981 Yuan W, Luo Y, Liang S et al. (2011) Thermal adaptation of net ecosystem exchange.
982 *Biogeosciences*, **8**, 1453–1463.

983 Yuan W, Liu S, Zhou G et al. (2007) Deriving a light use efficiency model from eddy covariance
984 flux data for predicting daily gross primary production across biomes. *Agricultural and*
985 *Forest Meteorology*, **143**, 189–207.

986

Supporting information

Fig. S1: Friction velocity and landscape and wetland net ecosystem CO_2 exchange.

Fig. S2: Wind direction and landscape and wetland net ecosystem CO_2 exchange.

Fig. S3: Daily gross primary production (GPP), ecosystem respiration (ER), and net ecosystem CO_2 exchange (NEE)

Fig. S4: Air temperature and soil temperature, incoming shortwave radiation, and snow depth and daily liquid precipitation.

Fig. S5: Daily air temperature at Fort Simpson versus daily air temperature from regional climate/earth system model simulations.

Fig. S6: Projected end-of-the-21st-century changes in near-surface air temperature, incoming shortwave radiation, and precipitation compared to the current conditions.

Fig. S7: Projections of modeled monthly wetland gross primary productivity, ecosystem respiration, and net ecosystem carbon dioxide exchange at Scotty Creek.

Fig. S8: Current analogues of the projected end-of-the-21st-century climate at Scotty Creek for the RCP4.5 scenario and for the RCP8.5 scenario.

Fig. S9: Net ecosystem CO_2 exchange from five Earth System Model simulations from the Coupled Model Intercomparison Project (CMIP5) for the grid cell comprising Scotty Creek (61°18' N; 121°18' W).

Fig. S10: Mean monthly and mean annual net ecosystem CO_2 exchange from CarbonTracker and five ESMs for the period 2006 to 2015 for the grid cell comprising Scotty Creek.

Tab. S1: Best fit parameters for the models of gross primary productivity and ecosystem respiration at the landscape- and the wetland-scale.

Tab. 1: Mean daily net ecosystem CO_2 exchange (NEE_{LAND}), gross primary productivity (GPP_{LAND}), and ecosystem respiration (ER_{LAND}) at landscape-level (± one standard deviation) for 5 °C-daily air temperature (T_a) bins between 23 March 2015 and 30 August 2016. Number of days (*n*) for bins for the observation period at Scotty Creek and the percentage of days with T_a within the bins at Fort Simpson between 2006 and 2015 (data from: Environment Canada, 2016; http://climate.weather.gc.ca/climate_data/).

	NEE_{LAND} ± std µmol m^{-2} s^{-1}	GPP_{LAND} ± std µmol m^{-2} s^{-1}	ER_{LAND} ± std µmol m^{-2} s^{-1}	*n*	*days* *%*
$T_a \leq$ -2.5 °C	+0.28±0.22	0.04±0.11	0.33±0.17	169	45.6
-2.5 °C < $T_a \leq$ 2.5 °C	+0.28±0.27	0.21±0.19	0.49±0.22	53	8.5
2.5 °C < $T_a \leq$ 7.5 °C	+0.16±0.56	0.72±0.68	0.88±0.62	52	9.1
7.5 °C < $T_a \leq$ 12.5 °C	-0.45±0.65	2.26±1.32	1.81±1.03	63	10.5
12.5 °C < $T_a \leq$ 17.5 °C	-0.67±0.85	3.74±1.40	3.08±1.06	90	15.2
17.5 °C < $T_a \leq$ 22.5 °C	-0.80±0.58	4.35±1.32	3.55±1.07	86	9.8
$T_a >$ 22.5 °C	-0.59±0.52	5.15±0.59	4.56±0.74	12	1.3

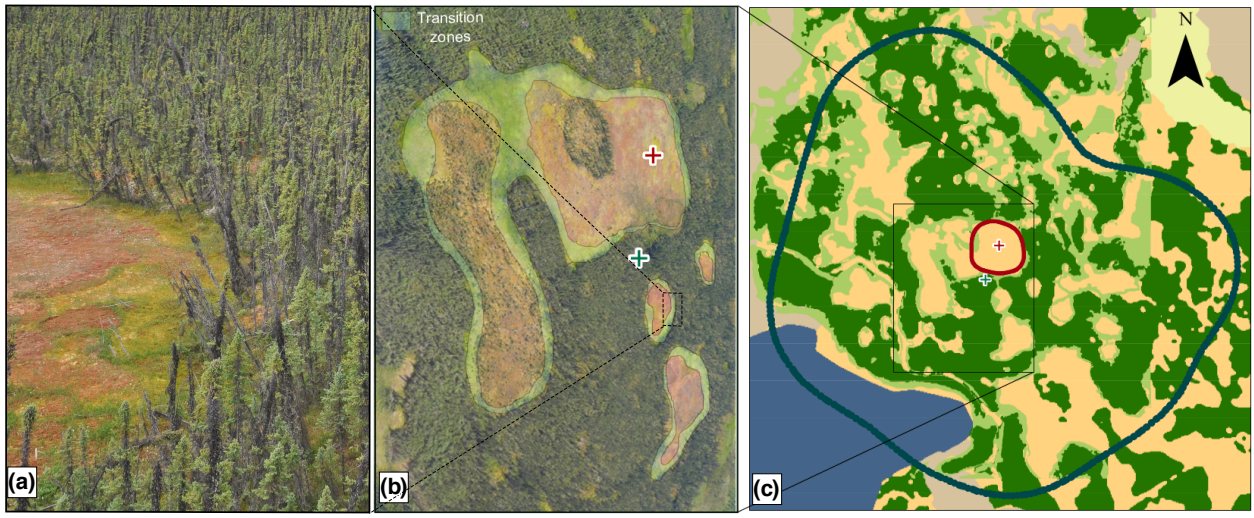

Fig. 1: **(a)** Oblique photograph of an actively thawing transition zone between wetland and forest. **(b)** Oblique photograph of the studied boreal forest-wetland landscape taken from a helicopter. Bright green areas represent visually delineated transition zones (several metres in lateral extent). **(c)** Land cover types in the flux footprints of the wetland (red cross) and the landscape tower (green cross): forested permafrost peat plateaus (dark green) and wetlands [collapse-scar bogs (yellow), fens (light brown), and an upland on post-glacial till (greenish yellow in the top right corner, outside the footprint)]. Wetland areas that have been converted from forested permafrost peat plateaus since 1977 (transition zones as identified using historical aerial photographs) are indicated in light green. Note that the extent of the transition zone map in **(c)** is limited to the east and south. Solid lines show landscape (dark green) and wetland tower (red) 90 % flux footprint climatology.

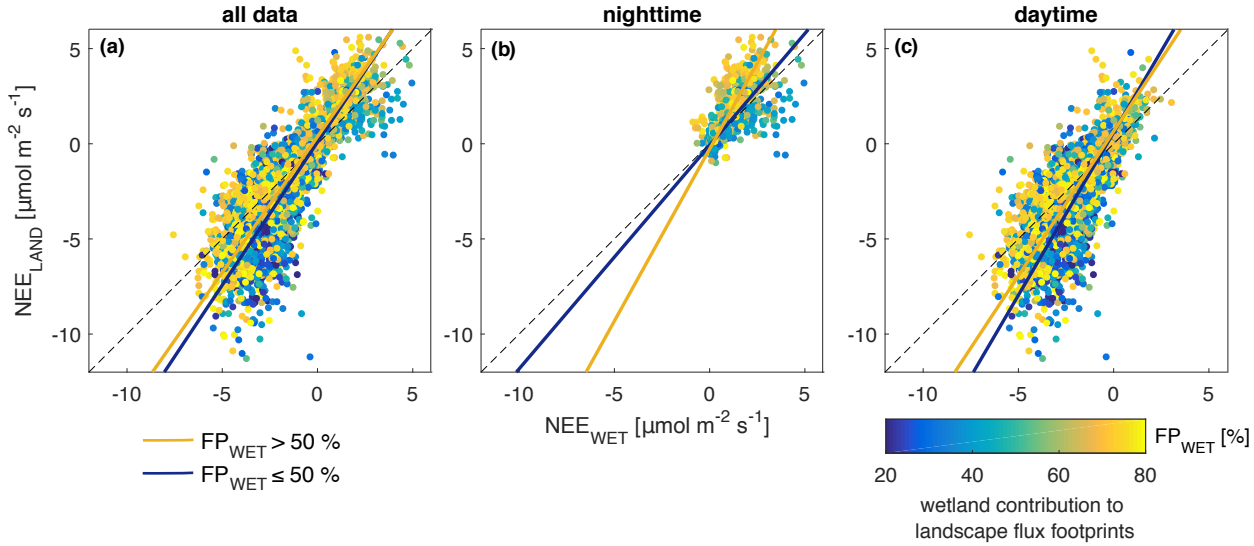

Fig. 2: Comparison of half-hourly net ecosystem carbon dioxide exchange at the landscape- (NEE_{LAND}) and wetland-scale (NEE_{WET}) for **(a)** all, **(b)** only nighttime, and **(c)** only daytime measurements. Data points are color-coded according to the wetland contribution to landscape flux footprints (FP_{WET}). The solid blue and yellow lines show the total least squares regressions for low (FP_{WET} < 50 %) and high FP_{WET} ($FP_{WET} \geq 50$ %), respectively.

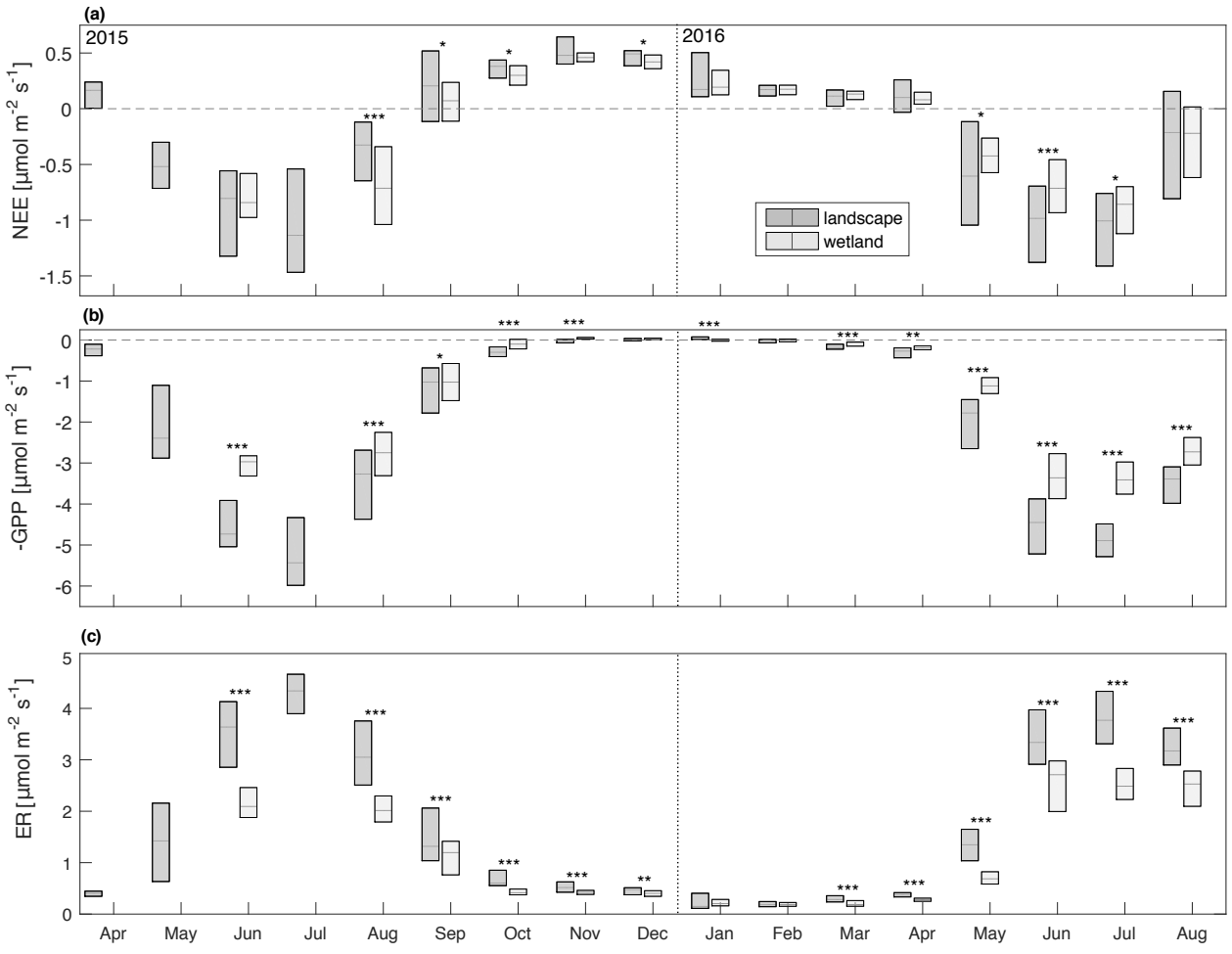

Fig. 3: **(a)** Daily net ecosystem carbon dioxide exchange (NEE), **(b)** gross primary productivity (GPP), and **(c)** ecosystem respiration (ER) from the wetland and landscape (including wetlands and forests) tower for individual months. Boxes show 25th and 75th percentiles; grey lines inside the boxes show medians. Monthly medians with asterisks are significantly different (Wilcoxon signed-rank test; * $\alpha = 0.05$ / ** $\alpha = 0.01$ / ** $\alpha = 0.001$). Note that data from the wetland tower is missing for April, May, and July 2015 due to sensor malfunctioning.

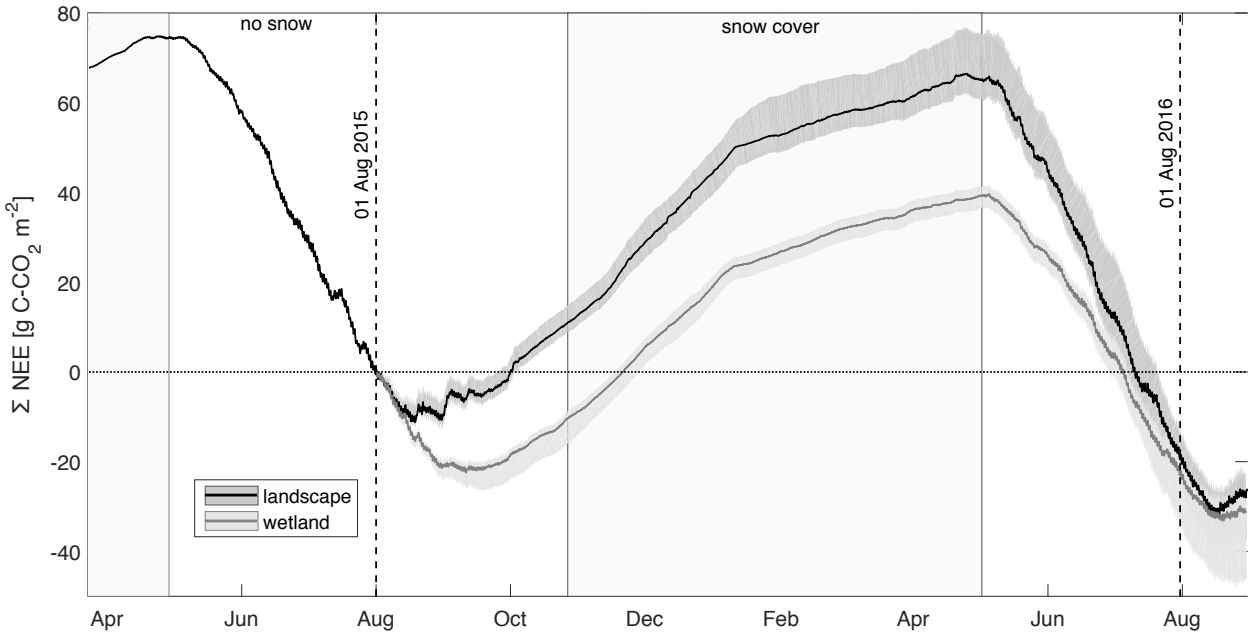

Fig. 4: Cumulative gap-filled net ecosystem carbon dioxide exchange at the landscape- and wetland-scale (ΣNEE_{LAND} & ΣNEE_{WET}, solid lines). Grey shaded areas indicating 95 % confidence intervals of ΣNEE between August 2015 and 2016 due to the friction velocity threshold and random errors in NEE measurements.

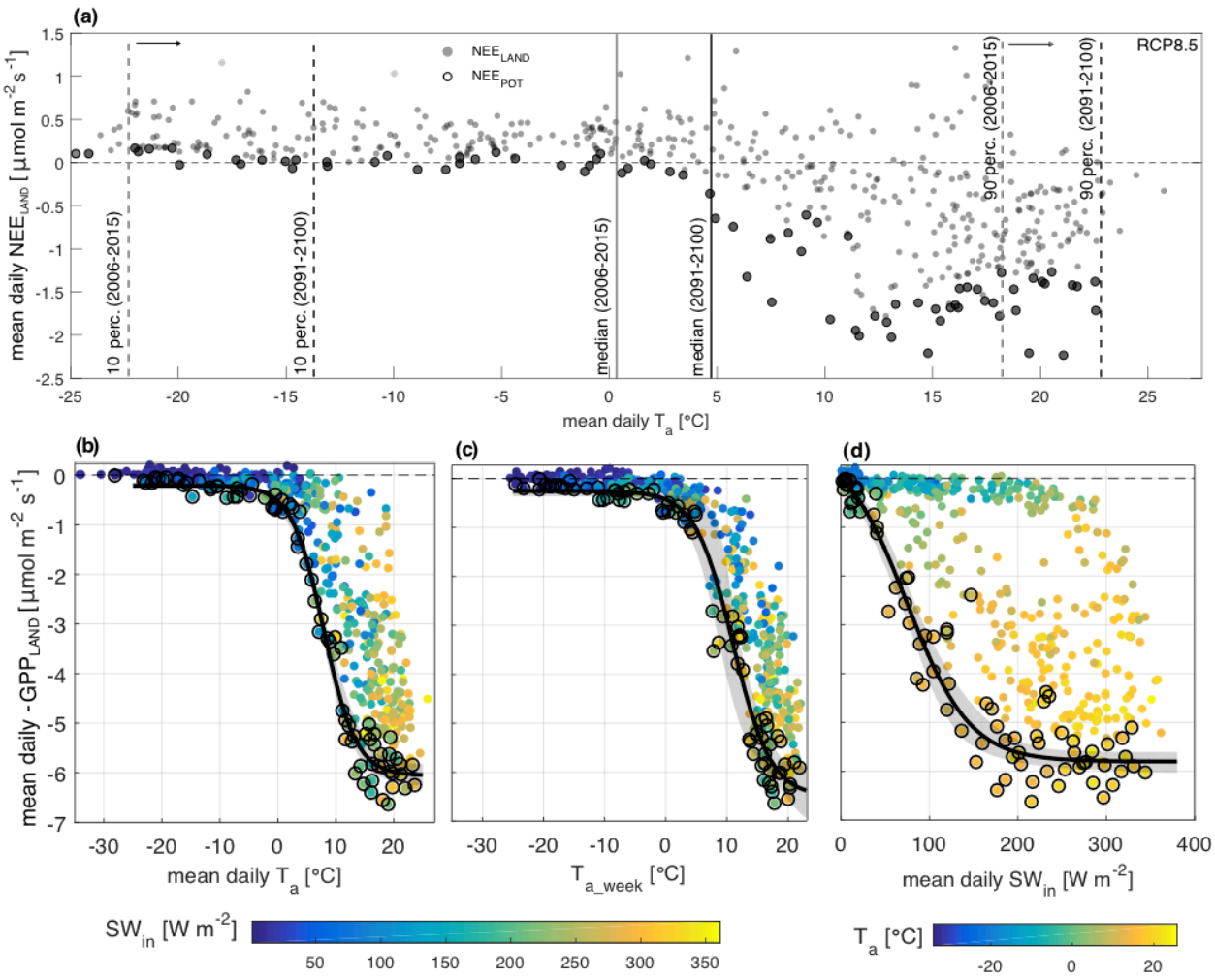

Fig. 5: **(a)** Mean daily air temperature (T_a) and net ecosystem carbon dioxide exchange at the landscape tower (NEE_{LAND}). Closed circles show measured NEE_{LAND} and open circles show potential NEE. Solid lines indicate the current and projected median of daily T_a between 2006-2015 and 2091-2100. Dashed lines show the respective 10^{th} and 90^{th} percentiles. Mean daily gross primary productivity derived from NEE_{LAND} (GPP_{LAND}) against **(b)** mean daily T_a and **(c)** the seven-day moving average of T_a. Solid lines are best model fits to potential GPP (circles) and shaded areas indicate the 95 % confidence interval. Color-coding of data points represents mean daily incoming shortwave radiation (SW_{in}). (d) GPP_{LAND} against SW_{in}. Color-coding shows T_a.

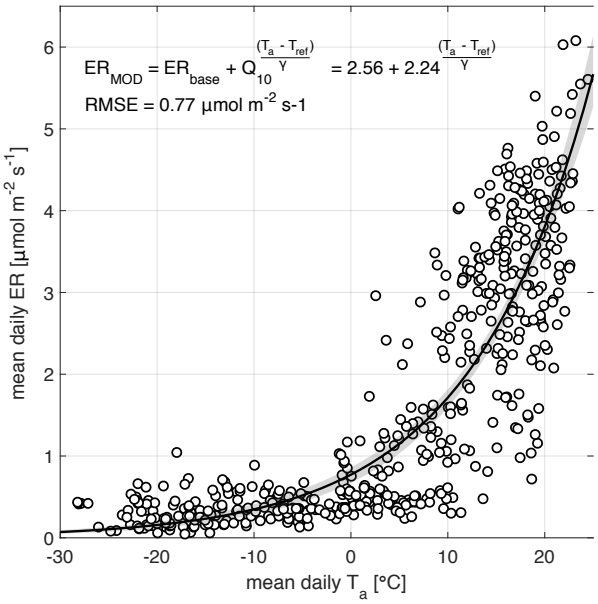

Fig. 6: Mean daily ecosystem respiration at the landscape tower (ER_{LAND}) against mean daily T_a. Solid line shows the best-fit Q_{10}-model.

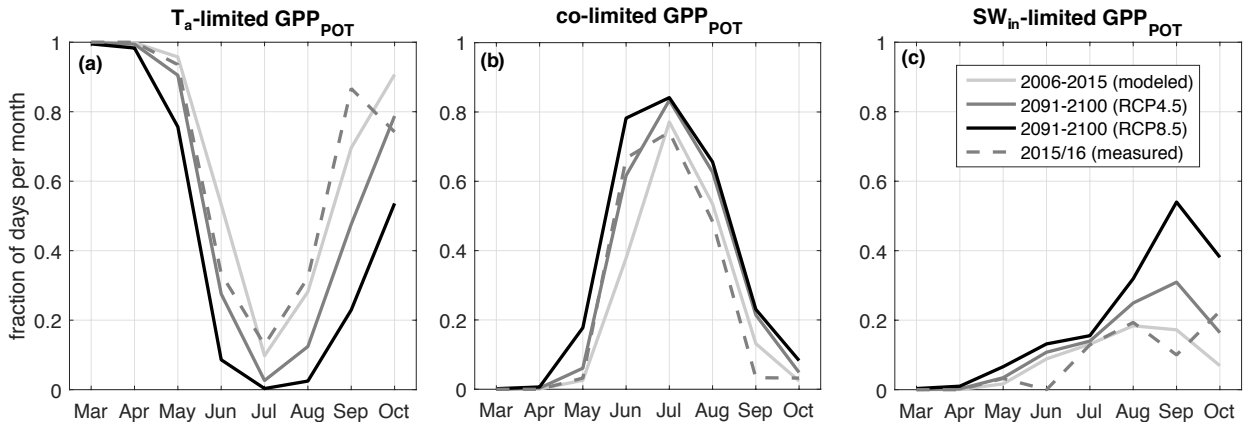

Fig. 7: Monthly fraction of days when potential gross primary productivity (GPP_{POT}) is limited by **(a)** air temperature (T_a), **(c)** incoming shortwave radiation (SW_{in}), or **(b)** co-limited by both variables. The dashed line shows GPP_{POT}-limitation for T_a and SW_{in} measured at Scotty Creek between August 2015 and July 2016. Solid lines indicate ensemble mean GPP_{POT}-limitation for the recent and projected modeled T_a and SW_{in} from six combinations of four regional and three global climate models.

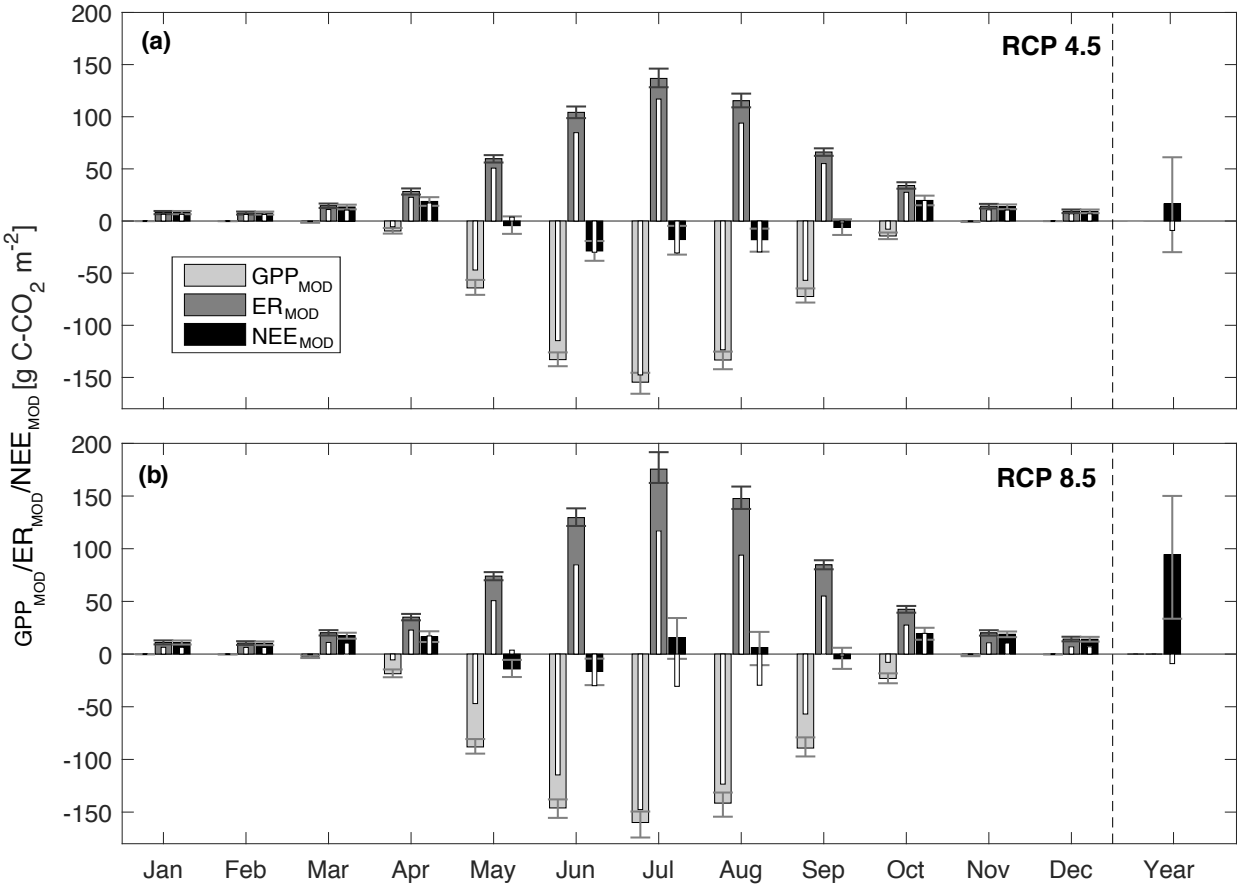

Fig. 8: Projections (2091-2100) of monthly modeled gross primary productivity (GPP_{MOD}), ecosystem respiration (ER_{MOD}), and net ecosystem carbon dioxide exchange (NEE_{MOD}) for the landscape at Scotty Creek **(a)** for the RCP 4.5 and **(b)** for the RCP 8.5 scenario. For comparison, narrow white bars show recent (2006-2015) GPP_{MOD}, ER_{MOD}, and NEE_{MOD}. Error bars indicate uncertainties (95 % confidence intervals) in the GPP- and ER-model.

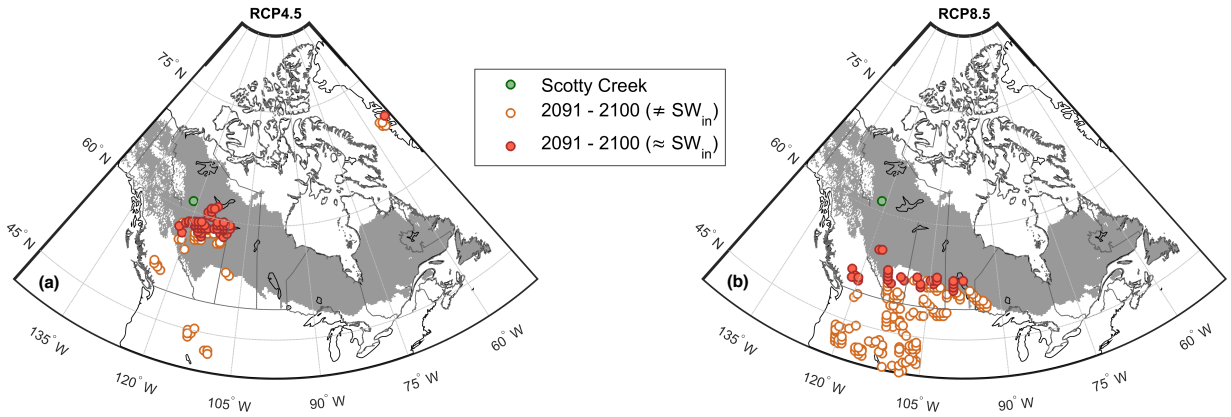

Fig. 9: Current climate analogues (2006-2015) of the projected end-of-21st-century (2091-2100) climate at Scotty Creek **(a)** for the RCP4.5 scenario and **(b)** for the RCP8.5 scenario. Circles show all climate analogues from six different regional/global climate model combinations. The green circle indicates the location of Scotty Creek. Orange circles show locations of current climates similar to the projected climate for Scotty Creek (±10 % difference in mean annual precipitation and ±0.5 °C of mean annual air temperature). Red circles indicate locations where, additionally, differences in annual incoming shortwave radiation (SW_{in}) are ±30 %. Grey shaded area is the current extent of the boreal zone (data from Brandt, 2009).